Assessing chromophoric dissolved organic matter (CDOM) distribution, stocks, and fluxes in Apalachicola Bay using combined field, VIIRS ocean color, and model observations

Ishan D. Joshi [a], Eurico J. D'Sa [a,*], Christopher L. Osburn [b], Thomas S. Bianchi [c], Dong S. Ko [d], Diana Oviedo-Vargas [b], Ana R. Arellano [c], Nicholas D. Ward [c,e]

[a] Department of Oceanography and Coastal Sciences, Louisiana State University, Baton Rouge, LA 70803, USA
[b] Department of Marine Earth and Atmospheric Sciences, North Carolina State University, Raleigh, NC 27695, USA
[c] Department of Geological Sciences, University of Florida, Gainesville, FL 32611, USA
[d] Oceanography Division, Naval Research Laboratory, Stennis Space Centre, MS 39529, USA
[e] Whitney Laboratory for Marine Bioscience, University of Florida, St. Augustine, FL 32080, USA

ARTICLE INFO

ABSTRACT

Understanding the role of estuarine-carbon fluxes is essential to improve estimates of the global carbon budget. Dissolved organic matter (DOM) plays an important role in aquatic carbon cycling. The chromophoric fraction of DOM (CDOM) can be readily detected *via in situ* and remotely-sensed optical measurements. DOM properties, including CDOM absorption coefficient at 412 nm (a_g412) and dissolved organic carbon (DOC) concentrations were examined in Apalachicola Bay, a national estuarine research reserve located in the northeast Gulf of Mexico, using *in situ* and satellite observations during the spring and fall of 2015. Synoptic and accurate representation of estuarine-scale processes using satellite ocean color imagery necessitates the removal of atmospheric contribution (~90%) to signals received by satellite sensors to successfully link to *in situ* observations. Three atmospheric correction schemes (*e.g.,* Standard NIR correction, Iterative NIR correction, and SWIR correction) were tested first to find a suitable correction scheme for the VIIRS imagery in low to moderately turbid Apalachicola Bay. The iterative NIR correction performed well, and validation showed high correlation ($R^2 = 0.95$, $N = 25$) against *in situ* light measurements. A VIIRS-based CDOM algorithm was developed ($R^2 = 0.87$, $N = 9$) and validated ($R^2 = 0.76$, $N = 20$, RMSE = 0.29 m^{-1}) against *in situ* observations. Subsequently, a_g412 was used as a proxy of DOC in March (DOC = $1.08 + 0.94 \times a_g412$, $R^2 = 0.88$, $N = 13$) and in November (DOC = $1.61 + 1.33 \times a_g412$, $R^2 = 0.83$, $N = 24$) to derive DOC maps that provided synoptic views of DOC distribution, sources, and their transport to the coastal waters during the wet and dry seasons. The estimated DOC stocks were ~3.71×10^6 kg C in March and ~4.07×10^6 kg C in November over an area of ~560 km^2. Volume flux (out of the bay) almost doubled for March 24 (735 m^3 s^{-1}) relative to November 4 (378 m^3 s^{-1}). However, estimates of DOC fluxes exported out of the bay from model-derived currents and satellite-derived DOC were only marginally greater in March (0.163×10^6 kg C d^{-1}) than in November (0.124×10^6 kg C d^{-1}) and reflected greater DOC stocks in the fall. The combination of satellite-, field-, and model-based observations revealed the strong linkage between the Apalachicola River plume, a major source of DOM, and the overall hydrodynamic forcing that controlled distributions of CDOM abundance, DOC concentration, stocks, and fluxes in the bay.

1. Introduction

Estuaries represent transitional/critical zones between terrestrial and marine environments (Bianchi, 2007). Dissolved organic matter (DOM) derived from the terrestrial environment is an important source of dissolved organic carbon (DOC) to coastal oceans often modified by biotic and abiotic processes during transport before its eventual arrival to the coastal waters. Roughly 15 to 25 Pg of DOC is produced annually *via* allochthonous and autochthonous processes in coastal ecosystems and transported to the world's oceans (Bauer and Bianchi, 2011). These processes include microbial activity (McCarthy et al., 1998), atmospheric diffusion (Jurado et al., 2008), subterranean groundwater discharge (Santos et al., 2009), river discharge (Hedges et al., 1992; Jaffé et al., 2004), and resuspension of bottom sediments (Hansell and Carlson, 2014). The roles of allochthonous and autochthonous DOC have been widely studied using field observations for investigating source and sink processes, examining spatial and temporal distributions,

* Corresponding author.
E-mail address: ejdsa@lsu.edu (E.J. D'Sa).

and estimating estuarine-DOC transport to adjacent coastal waters in various regions of the globe (Bianchi et al., 2009; Fellman et al., 2009; Fichot and Benner, 2014; Huguet et al., 2009; Moyer et al., 2015; Osburn et al., 2016; Sleighter and Hatcher, 2008). Although *in situ* observations have been widely used, they provide limited spatial and temporal coverage. Satellite remote sensing with its synoptic and repeated coverage over large regions, has the potential to greatly enhance our ability to monitor the processes controlling aquatic DOC cycling, particularly in coastal and estuarine environments (Bauer et al., 2013; Borges et al., 2005).

Chromophoric dissolved organic matter (CDOM) is an optically-active fraction of the DOM pool that is characterized by increasing light-absorption towards the UV–visible wavelengths (Green and Blough, 1994; Kirk, 1994). The optical characteristics of CDOM (*e.g.*, absorption coefficients and spectral slopes) are well-known proxies for variations in DOM molecular weight corresponding to DOM sources and photo-chemical history (Brown, 1977; D'Sa et al., 2014; Fichot and Benner, 2012; Helms et al., 2008). Several studies have demonstrated the possible use of CDOM absorption coefficients to assess DOC concentration using a conservative CDOM-DOC relationship in a variety of coastal waters (Del Castillo and Miller, 2008; Del Vecchio and Blough, 2004; Fichot and Benner, 2011; Spencer et al., 2007; Vantrepotte et al., 2015). Numerous studies have proposed the use of ocean color sensors to assess CDOM in estuarine and coastal waters (D'Sa, 2008; D'Sa and Miller, 2003; Loisel et al., 2014). This has allowed for linkages between satellite-estimated CDOM and *in situ* CDOM-DOC relationships, which can be used to elucidate DOM distributions and estuarine-scale processes in the context of global carbon reserves with high spatiotemporal resolution (Chaichitehrani et al., 2014; Joshi and D'Sa, 2015; Loisel et al., 2014; Mannino et al., 2008; Tehrani et al., 2013). Furthermore, combining satellite remote sensing data with numerical hydrodynamic model results can be used to gain better insights on the linkages between physical processes and the distribution and transport of water constituents of interest in the coastal environments (D'Sa and Ko, 2008; Lehrter et al., 2013).

Apalachicola Bay, a national estuarine research reserve located in the northeast Gulf of Mexico, is well-known for its high water quality and oyster yields (Edmiston, 2008a; Whitfield and Beaumariage, 1977; Wilber, 1992). Although studies of suspended particulate organic matter distribution under different weather conditions and biophysical phenomena have been undertaken (Chen et al., 2011a; Chen et al., 2011b; Huang et al., 2002b; Liu and Huang, 2009), the DOM component has not been investigated in the bay. The main aim of this study was to evaluate the applicability of recently launched Visible Infrared Imaging Radiometer Suite (VIIRS) sensor for monitoring CDOM and DOC concentrations in Apalachicola Bay, obtaining synoptic views of their distributions, potential sources, and transport mechanisms to shelf waters, and initiating efforts to recognize the contribution of the Apalachicola estuary to North American carbon budgets. The main objectives of this study were as follows: 1) finding a suitable atmospheric-correction scheme for the VIIRS imagery due to large atmospheric contributions (~ 90%) to the at-sensor radiance thus minimizing uncertainties of the water-leaving radiance; 2) developing a VIIRS-based CDOM empirical algorithm, and CDOM-DOC relationships for Apalachicola Bay to generate CDOM and DOC maps; 3) examining major forcing factors (*e.g.*, winds, tides, and rivers) and their effects on spatial and seasonal distributions of CDOM and DOC using combined field, satellite, and modeling observations; and 4) estimating DOC stocks and fluxes during two field surveys in Apalachicola Bay.

2. Methods and materials

2.1. Study area

Apalachicola Bay is a relatively shallow (average depth = ~3.0 m) bar-built estuary, located in the Florida Panhandle, that covers an area

of about 542 km^2 (Fig. 1). High river discharge, shallow water depths, and multiple connections to the open Gulf allow for dynamic interactions between local and far-field wind/tidal effects in this estuarine system (Schroeder and Wiseman, 1999). In fact, this highly dynamic physical forcing results in Apalachicola Bay having one of the shortest water residence times (*ca.* 10 days) among all estuaries in the Gulf of Mexico (Solis and Powell, 1999). As one of the most productive natural systems in North America, the bay is well recognized by the state, federal and international organizations for its pristine water-quality and healthy ecosystem (Edmiston, 2008a). The deltaic processes of the Apalachicola River, relatively unpolluted alluvial system and major source of freshwater, shaped the modern appearance of the bay and surrounding barrier islands. Relatively fresh bay and saline Gulf waters exchange through the Indian Pass, the East Pass, the West Pass, and a man-made navigational channel called Sike's Cut (Fig. 1). Apalachicola Bay is also known for its oyster harvest that supplies ~90% of the total oyster yield in Florida, and accounts for ~10% of the nationwide oyster production (Whitfield and Beaumariage, 1977; Wilber, 1992). In recent times, the bay's oyster harvest has been negatively affected by various environmental stressors, *e.g.*, salt-water intrusion (Havens et al., 2013), tropical storms (Edmiston et al., 2008b), the Deep Water Horizon oil spill (Grattan et al., 2011), and droughts and floods (Livingston, 2014; Livingston et al., 1997). Apalachicola Bay is located at an important transitional zone, where diurnal tides of the western Gulf change to semi-diurnal tides towards the Florida Panhandle (Huang et al., 2002b; Koch and Sun, 1999). It also experiences mostly low to moderate winds with short periods of strong winds during extreme weather events, such as cold fronts and hurricanes that can have large effects on the bay's water quality (Chen et al., 2009; Liu and Huang, 2009).

2.2. Sample and data collection

Surface water samples were collected during two field surveys in March and November 2015 (Fig. 1). In March, seventeen stations (orange symbols) were sampled from Central Bay, East Bay, and St. George Sound for remote sensing analysis, while same and additional 9 stations (purple symbols) were sampled in November. Surface temperature and salinity were recorded *in situ* using a handheld Yellow Springs Instruments (YSI) Professional Plus multi-probe field meter. Surface water samples were filtered immediately following collection. Samples were stored in the dark on ice during transport to laboratory that same day. The samples were filtered using pre-rinsed 0.2-μm porosity Nuclepore membrane filters (Whatman GmbH), and measured for the optical absorption within two days. Water samples were also filtered using pre-combusted Whatman 0.7-μm porosity GFF filters ($\Phi = 47$ mm) into a combusted glass flask for dissolved organic carbon (DOC) analysis. Meteorological observations (air temperature, wind speed, and wind direction) were obtained from the East Bay station (29.791°N, −84.883°W, *Apalachicola National Estuarine Research Reserve* (ANERR); white star in Fig. 1) for examining the effects of meteorological factors on distribution of the DOM properties (*e.g.*, CDOM absorption coefficient and DOC). Salinity time-series was obtained at ANERR-maintained Cat Point (CP) and Dry Bar (DB) stations to study river plume dynamics and tidal-influence during the satellite overpass (Fig. 1). Water level and tidal-height were obtained from a tidal station located in East Bay (ID-8728690, 29.435°N, −84.90°W; *NOAA Tide and Currents*). Apalachicola River discharge, measured near Sumatra, Florida (blue star in Fig. 1), was acquired from the *USGS* water data archive (www.waterdata.usgs.gov) to study effects of season-dependent riverine inputs on the DOM properties in Apalachicola Bay. Above-water measurements of water-surface radiance (L_{target}), sky radiance (L_{sky}), and reference-plate radiance (L_{plate}) were collected using *GER1500* spectroradiometer under clear-sky conditions (Mobley, 1999). The spectroradiometer was set to provide an average of 4 internal scans by considering the variability in reference and target conditions. Consequently, the final spectrum was an average of 12 spectra (3 replicates with 4 internal scans per
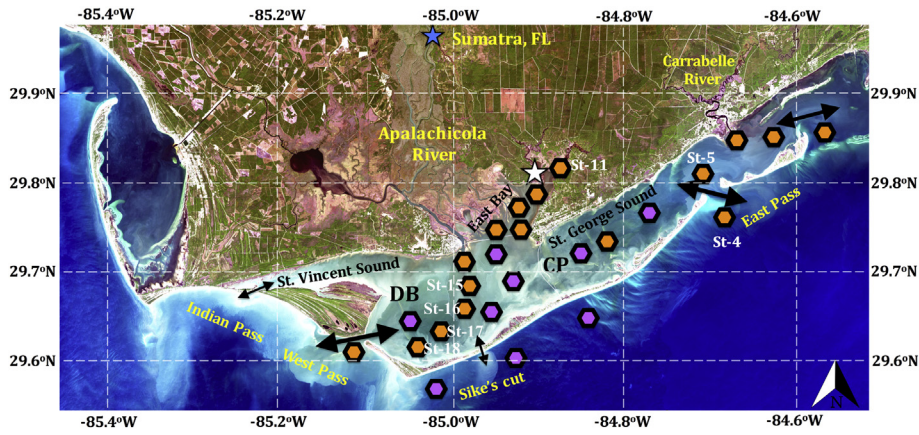
Fig. 1. Apalachicola Bay, Florida (USA). *In situ* measurements acquired at 17 stations on March 23–25, 2015 (orange symbols) with nine stations further added on November 2–4, 2015 (purple symbols). Blue and white stars illustrate hydrological and meteorological stations, respectively. CP and DB are the ANERR-maintained salinity stations, Cat Point and Dry Bar, respectively. The arrows indicate the open boundaries between the bay and shelf waters that were used to calculate the fluxes. (For interpretation of the references to color in this figure legend, the reader is referred to the web version of this article.)

measurement) at each sampling station. Glint and residual corrections were applied on raw radiance measurements as suggested by Gould et al. (2001). The level-L1B VIIRS (Visible Infrared Imaging Radiometer Suite) imagery (Sensor Data Record-SDR product) was downloaded from NASA's Ocean Color website, and processed using SeaDAS 7.3 (OBGP, NASA).

Radiometrically-calibrated VIIRS imagery was converted into the CDOM absorption coefficient a_g412 and DOC concentration maps using two pathways (Fig. 2): 1) evaluating and applying a suitable atmospheric-correction scheme to the VIIRS imagery in an optically complex coastal system, and 2) developing empirical relationships between atmospherically-corrected R_{rs} and a_g412, and subsequently to DOC concentration to convert the VIIRS imagery into the a_g412 and DOC maps for Apalachicola Bay.

2.3. Absorption spectroscopy

Absorbance (A) spectra were measured on a Perkin Elmer Lambda-850 double beam spectrophotometer equipped with a 150 mm-integrating sphere. Following the instrument warm up and equilibration of samples to room temperature, absorbance spectra were obtained between 250 and 750 nm at 1-nm intervals using 10-cm path length quartz cuvette. The cuvette was rinsed twice with ultrapure water (a Thermo Scientific Micro-Pure UV purification system with a purity of 18.2 MΩ) and once with filtered seawater before each measurement

to avoid contamination by the previous sample. Absorption coefficients (a_g) were calculated using the following equation,

$$a_g(\lambda) = 2.303 \times \frac{A(\lambda)}{L} \tag{1}$$

where, A(λ) is absorbance at a wavelength λ, and L is pathlength in meters. The absorption spectra were corrected for scattering, temperature, and baseline drift by subtracting a value of absorption at 750 nm from each spectrum (Green and Blough, 1994). Wavelength-dependent exponential decay of the absorption coefficient can be given by the following non-linear equation,

$$a_g(\lambda) = a_g(\lambda_{ref}) \times e^{-S(\lambda - \lambda_{ref})} \tag{2}$$

where, $a_g(\lambda)$ is the amplitude of the CDOM absorption coefficient at any wavelength λ, and λ_{ref} is the reference wavelength (Jerlov, 1976; Shifrin, 1988). The absorption spectra generally represented by a non-linear equation (Eq. (2)), were converted to a linear form by a logarithmic transformation of dependent variable. Then, a least squares regression approach was applied to calculate spectral slope S (μm^{-1}) between 275 nm and 295 nm ($S_{275-295}$), while absorption coefficient at 412 nm (a_g412) was used as a quantitative parameter of the CDOM (D'Sa et al., 2006; D'Sa et al., 2014).
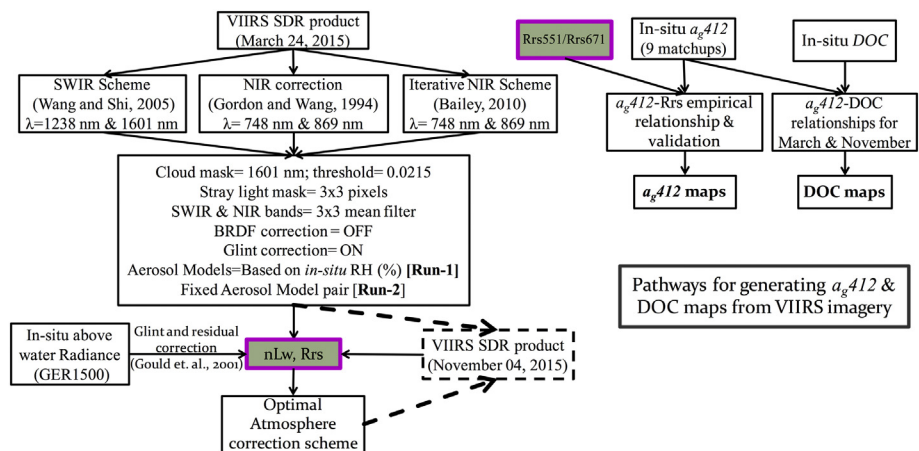

Fig. 2. Processing-approach to generate the a_g412 and DOC maps using the VIIRS imagery and *in situ* measurements in Apalachicola Bay.

2.4. DOC analysis

Dissolved organic carbon (DOC) was measured on an OI Analytical 1030D TOC analyzer using wet chemical oxidation (sodium persulfate) modified for seawater analyses (Osburn and St-Jean, 2007). Milli-Q laboratory water (18.2 MΩ; <10 µg C L^{-1} TOC) was used to prepare standards and reagents and as a blank. Calibration of the instrument was achieved daily using solutions of caffeine (0 to 20 mg C L^{-1}). Reproducibility of this system is 5% RSD (relative standard deviation). Routine measurement of Hansell Certified Reference Material (CRM) DOC standards with each analytical run resulted in DOC values of 0.54 ± 0.07 mg C L^{-1}.

2.5. Above-water measurements

In situ water-surface radiance (L_{target}, N = 40–50°, A = 90°–135°), sky radiance (L_{sky}, Z = 40°–50°, A = 90°–135°), and reference-plate radiance (L_{plate}, N = 0°, A = 90°–135°) (N = nadir angle, Z = zenith angle, A = azimuth angle from solar plane) were converted to downwelling irradiance (E_d), remote-sensing reflectance (R_{rs}), and normalized water-leaving radiance (nL_w) using the following equations (Mueller et al., 2003):

$$\text{Downwelling Irradiance } (E_d) = \pi \times \frac{L_{plate}}{\rho_{plate}} \left(Wcm^{-2}nm^{-1} \times 10^{-10} \right) \quad (3)$$

$$\text{Remote Sensing Reflectance } (R_{rs}) = \frac{L_{target} - \left(\rho \times L_{sky} \right)}{E_d} - R_{rs}(residual) \quad (4)$$

$$\text{Normalized water leaving radiance } (nL_w) \approx R_{rs} \times F_0 \ (mWcm^{-2}\mu m^{-1}sr^{-1}) \quad (5)$$

where, L_{target} = target radiance in ($Wcm^{-2}nm^{-1}sr^{-1} \times 10^{-10}$), L_{plate} = reference-plate radiance in ($Wcm^{-2}nm^{-1}sr^{-1} \times 10^{-10}$), L_{sky} = sky radiance in ($Wcm^{-2}nm^{-1}sr^{-1} \times 10^{-10}$), L_w = water-leaving radiance ($Wcm^{-2}nm^{-1}sr^{-1} \times 10^{-10}$), ρ_{plate} = reference-plate reflectance (10%), ρ = proportionality factor that relates total sky radiance to sea surface-reflected sky radiance, $R_{rs}(residual)$ = residual sky radiance and F_0 = nominal band extraterrestrial solar Irradiance ($mWcm^{-2}\mu m^{-1}$) (Thuillier et al., 2003). The L_{target}, also includes surface-reflected sky-light, that should be removed to get a better estimation of the water-leaving radiance (Eq. (4)). The residual skylight can be removed with a null correction at NIR wavelengths (usually at 750 nm) (Mobley, 1999; Mueller et al., 2003). However, an assumption of zero radiance at NIR wavelength may not be appropriate in turbid waters, as it can result in underestimation in visible especially at the blue wavelengths (Lee et al., 1997; Mueller et al., 2003). Skylight and residual corrections were applied using the glint-correction approach suggested by (Gould et al., 2001) (*path-1 in their study*). This approach removes skylight with a residual-correction using known values of water absorption at 715 and 735 nm rather than considering zero radiance at a NIR wavelength.

2.6. Atmospheric correction of VIIRS imagery

Two clear-sky images were available during the field surveys; one on March 24, and another on November 4, 2015. Level-L1B images were processed to remove the atmospheric-contribution using SeaDAS 7.3 (OBPG, NASA) (Fig. 2). Prior to using the atmospheric-corrected products in our analysis, we tested three standard atmospheric-correction schemes; 1) NIR correction-GW94 (Gordon and Wang, 1994), 2) Iterative NIR correction-BFW10 (Bailey et al., 2010; Stumpf et al., 2003), and 3) SWIR correction-WS05 (Wang and Shi, 2005), to evaluate their performance, and to find an effective scheme for Apalachicola Bay. The atmospheric-correction was applied on March 24, 2015 image using

the candidate-schemes and necessary *l2gen* (SeaDAS 7.3) processing parameters, *e.g.*, real-time ancillary data, a cloud mask (threshold = 0.0215 at 1601 nm) (Wang and Shi, 2006), a stray-light mask (3 × 3 filter), glint correction, and no BRDF correction (Fig. 2). The *l2gen* module contains 80 aerosol models (8 relative humidity and 10 size fractions) that were reduced to 20 models based on *in situ* relative humidity (RH) measured close to the satellite overpass (Ahmad et al., 2010; McCarthy et al., 2012). Using 20 aerosol models and necessary *l2gen* parameters, atmospheric-correction module was invoked as the first run (*Run-1*) that provided useful information about the dominant aerosol model pair in our study area. By assuming relatively homogeneous aerosol properties over a small study area (Hu et al., 2000), the atmospheric correction module was re-run (*Run-2*) using a fixed aerosol model pair (*Run-1*) to get the final outputs of R_{rs} and nL_w. Different chlorophyll concentrations were observed at distinct locations in the bay, *e.g.*, moderate to high close to river mouth and near the marshes while low to moderate in St. George Sound and Outer Bay on March 23–24, 2015 (Fig. 3a). Therefore, based on bay turbidity and chlorophyll distributions, three distinct regions were selected for atmospheric correction analysis: East Bay and Cat Point (white), Central Bay and Dry Bar (green), St. George Sound and Outer Bay (orange) (Fig. 3b). The R_{rs} from three correction schemes were then compared to each other, and to *in situ* measurements for 325 pixels distributed among these regions of the bay. The best-performing scheme was further analyzed and validated against the *in situ* measurements for its applicability in different seasons in Apalachicola Bay.

2.7. Statistical analysis

Matchup comparisons between satellite-derived estimates and *in situ* measurements of the DOM properties (a_g412 and DOC), R_{rs}, and
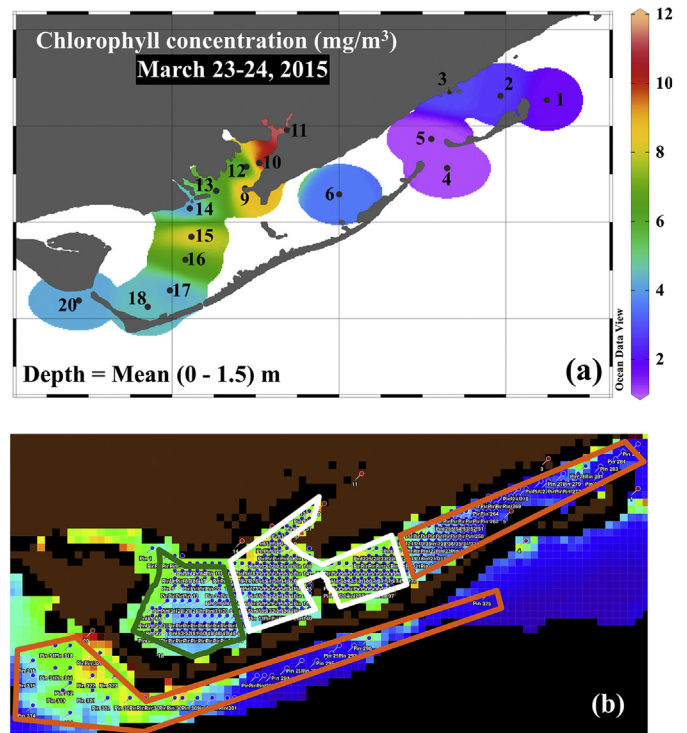

Fig. 3. (a) Surface chlorophyll concentrations (mg m^{-3}) in Apalachicola Bay on March 23–24, 2015, and (b) three atmospheric correction schemes are evaluated for 325 pixels in Apalachicola Bay. The pixels are divided among three regions as illustrated by orange (St. George Sound and Outer Bay), green (Central Bay and Dry Bar), and white (East Bay and Cat Point) colors corresponding to low, medium, and moderately turbid regions, respectively. (For interpretation of the references to color in this figure legend, the reader is referred to the web version of this article.)

nL_w were evaluated using statistical criteria, such as bias (%), root mean square error (RMSE), and R^2. R statistical software, MATLAB, and Sigma Plot (Systat Software Inc.) were used for data processing, descriptive statistics, and graphical-illustrations presented in this study.

2.8. NCOM model and flux calculations

A high-resolution (~250 m) estuarine model based on the Navy Coastal Ocean Model (NCOM) (Ko et al., 2008) that covers Apalachicola Bay is developed for this study. Estuarine circulation is mainly driven by tides and river flows and to a lesser extent by winds, evaporation and rainfall. Although the Apalachicola Bay is a semi-enclosed waterbody, its circulation is nevertheless connected to the open ocean and may have an impact from the encroaching Loop Current and Loop Current eddies. A northeastern Gulf of Mexico regional model with 1.5 km resolution, therefore, is applied to connect the deep Gulf to the coastal sea and then to Apalachicola Bay. The high-resolution estuarine model is forced with realistic tides, real-time river flows, wind and surface fluxes that include evaporation and rainfall from a high-resolution regional weather forecast model, the coupled ocean/atmosphere mesoscale predication system (COAMPS).

Hourly water volume transported (current, in m s^{-1}, × cross-sectional area, in m^2) in or out of the bay was obtained from the NCOM hydrodynamic model by integrating the flows around all the bay passes (e.g., Indian, West and East Passes; shown as arrows in Fig. 1). Hourly DOC flux rates over multiple tidal cycles were then computed by multiplying the satellite-derived DOC concentrations by the volume of water transported through the passes.

3. Results

3.1. Performance investigation of atmospheric correction schemes in Apalachicola Bay

Fig. 4 illustrates the Rayleigh-corrected surface reflectance ($\rho_{(TOA-Rayleigh)}$) at the NIR and SWIR wavelengths. The bay-water was relatively black ($\rho_{(TOA-Rayleigh)}$ ~ 0%) at SWIR wavelengths (1238 nm & 2257 nm) likely due to strong water absorption (Hale and Querry, 1973). However, the $\rho_{(TOA-Rayleigh)}$ increased only ~1–1.5% at NIR wavelength (862 nm), indicating low to moderately turbid nature of the bay even during high freshwater inputs on March 24, 2015.

The atmosphere contributes ~90% to the signal received by a satellite sensor; consequently the removal of atmospheric-contribution is a challenging, and yet necessary component of image processing in ocean color remote sensing (Gordon and Wang, 1994). Three well-known atmospheric-correction schemes were evaluated on a VIIRS image acquired on March 24, 2015, and validated against in situ measurements to find a suitable correction scheme for Apalachicola Bay. The performance of candidate-schemes (Fig. 5) was examined on 325 px in different parts of the bay as shown in Fig. 3. Gordon and Wang (1994; hereafter GW94) NIR scheme demonstrated negative R_{rs} in the blue, especially in the relatively turbid parts (e.g., green and white colors in Figs. 3 & 5a corresponding to Central and East Bays) of Apalachicola Bay; however, water-retrieval improved towards less turbid St. George Sound and shelf region just outside the bay (orange color). The SWIR-correction scheme (hereafter WS05) showed positive but strong signals of R_{rs} (410) throughout the bay and even in shelf waters. The iterative NIR-correction (BFW10) showed intermediate results between the GW94 and WS05 schemes, and also demonstrated a good agreement to the GW94 in relatively clearer shelf waters (orange region in Fig. 3 & 5a). Additionally, the BFW10 results correlated well with in situ observations at 410 nm indicating a reasonable performance of the iterative NIR-correction in relatively turbid Central Bay (green region in Figs. 3 & 5a).
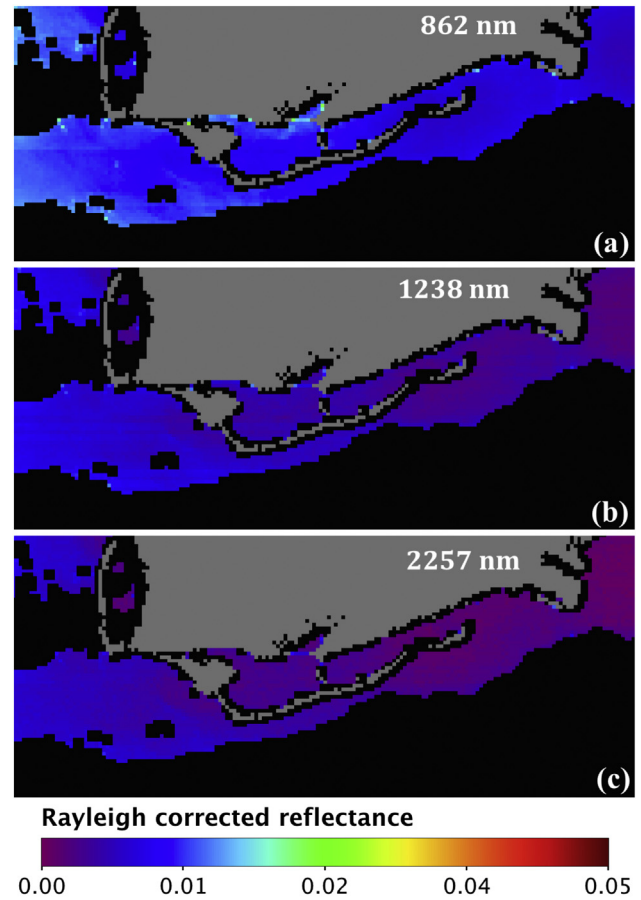

Fig. 4. Rayleigh-corrected surface reflectance at **a)** 862 nm, **b)** 1238 nm, and **c)** 2257 nm on March 24, 2015.
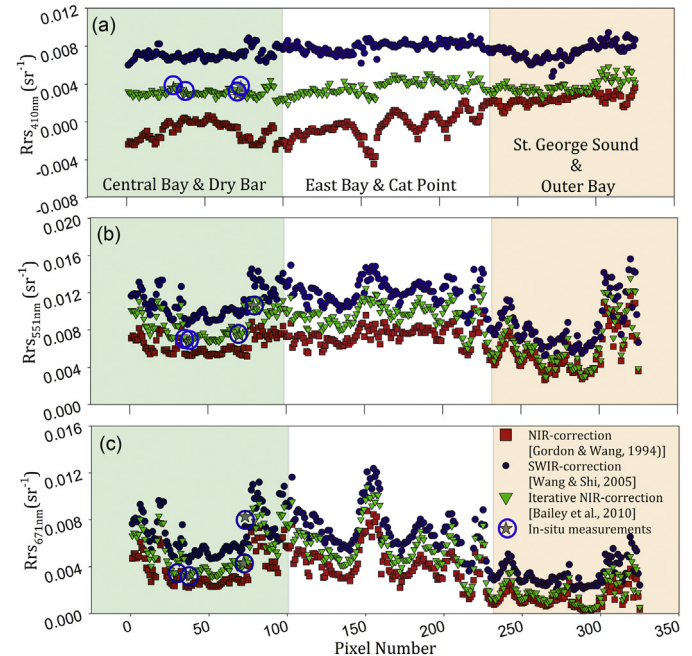

Fig. 5. An evaluation of three atmospheric-correction schemes; NIR-correction (Gordon and Wang, 1994), Iterative NIR-correction (Bailey et al., 2010), and SWIR-correction (Wang and Shi, 2005) on 325 pixels distributed among different regions (green, white, and orange polygons as in Fig. 3b) in Apalachicola Bay. Blue circle with grey stars indicate in situ measurements acquired on March 24, 2015. (For interpretation of the references to color in this figure legend, the reader is referred to the web version of this article.)

At 551 nm, the *BFW10* performed reasonably well, and showed a good agreement with *in situ* observations (Fig. 5b). The *GW94* and *WS10* schemes also approached towards the *BFW10* likely due to reduced atmospheric-correction errors near NIR and SWIR wavelengths, respectively. The agreement between all three schemes improved in clear-water pixels (orange region); yet relatively larger deviations were still observed in turbid-water pixels (green and white regions). At 671 nm, both the *GW94 and BFW10* schemes retrieved comparable estimates of R_{rs} (Fig. 5c), however, the *WS10* slightly deviated from the *BFW10* and *in situ* observations, possibly due to small but recognizable aerosol-correction errors (*e.g.*, aerosol model selection or absorbing aerosols) that could have propagated exponentially in general from SWIR to red wavelengths (McCarthy et al., 2012). This analysis showed that the iterative NIR-correction (*BFW10*) appeared to be the most suitable atmospheric-correction scheme for low to moderately turbid Apalachicola Bay.

Validity of the *BFW10* scheme was further tested against *in situ* observations (Fig. 6). *In situ* normalized water-leaving radiance (nL_w) correlated well with the *BFW10*-corrected VIIRS nLw (Fig. 6a), and R_{rs} spectra showed a good agreement at different stations in Central Bay during elevated river flow condition on March 24, 2015 (Fig. 6b). However, st-15 showed overall higher reflectance values compared to other stations, with a distinct reflectance peak at ~570 nm, a chlorophyll absorption trough at ~676 nm, and a fluorescence emission peak at ~685 nm, respectively. This station, located to the south of the river mouth, likely experienced increased turbidity due to a moderate river discharge (~700 m^3 s^{-1} on March 24, 2015) or re-suspended bottom sediments combined with an elevated chlorophyll concentration (~ 8 mg m^{-3}). The Iterative NIR scheme (*BFW10*) was further evaluated on November 4, 2015 that yielded R^2 = 0.95 (N = 25) during the low river flow condition (Fig. 6c). The iterative NIR-correction performed well overall in the different seasons (Fig. 6d). Although the satellite retrieval errors were relatively larger in the blue region, small errors in the green and the red channels suggested better suitability in using these bands for developing algorithms in Apalachicola Bay.

3.2. An empirical band-ratio algorithm and a_g412 – DOC relationships

In situ a_g412 measurements were regressed against various combinations of VIIRS-derived R_{rs} at blue (488 nm), green (551 nm), and red (671 nm) channels, and a green to red band-ratio showed a robust power-law relationship (R^2 = 0.87, N = 9) (Fig. 7a).

$$a_g412 \ (m^{-1}) = 3.184 \times \left(\frac{Rrs551}{Rrs671}\right)^{-1.046} \tag{6}$$

The validation results demonstrated a reasonable performance of the band-ratio algorithm that was improved further using a more constrained time difference (± 3 h) between the *in situ* measurements and the satellite overpass (Fig. 7b). Furthermore, a_g412 – DOC relationships developed from the field data were used to convert the satellite-derived CDOM to DOC in Apalachicola Bay. The DOC concentration in the bay was strongly correlated to a_g412 in March except close to the river and in East Bay, likely due to influences of the different *DOM* sources (*e.g.*, riverine DOM and wetland-derived blue carbon) at these locations (Eq. (7); Fig. 7c); whereas, it was well correlated to the a_g412 (Eq. (8)) throughout the bay in November possibly due to the dominance of a single *DOM* source within the bay.

$$DOC \ (mgL^{-1}) = 1.08 + 0.94 \times a_g412 \ (m^{-1}) \ [\text{March}] \tag{7}$$

$$DOC \ (mgL^{-1}) = 1.61 + 1.33 \times a_g412 \ (m^{-1}) \ [\text{November}] \tag{8}$$

The a_g412 and DOC were further studied using satellite-, field-, and model-based results to examine the effects of the meteorological, hydrological, and astronomical forcings on their sources and dispersal in Apalachicola Bay.
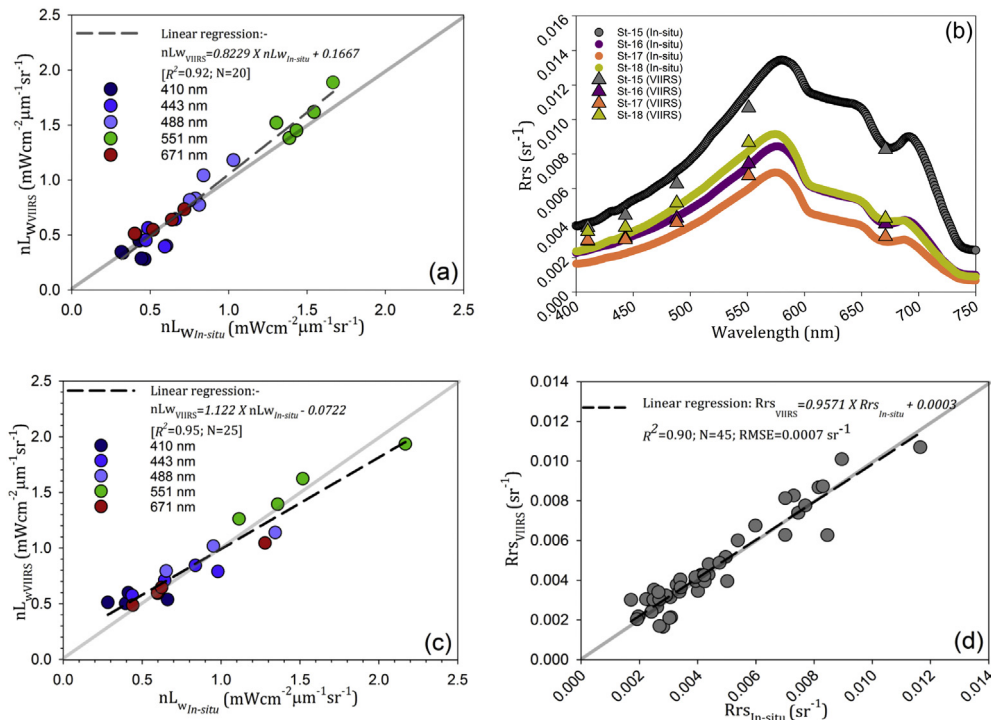

Fig. 6. Validation of iterative NIR (*BFW10*)-corrected nL_w and R_{rs} against *in situ* measurements. **a)** VIIRS nL_w vs. *in situ* nL_w on March 24, 2015 (R^2 = 0.92, N = 20, 4 stations in Central Bay), **b)** *In situ* R_{rs} spectra (circles) and VIIRS R_{rs} (triangles) on March 24, 2015, **c)** VIIRS nL_w vs. *in situ* nL_w on November 04, 2015 (R^2 = 0.95, N = 25, 5 stations in Central Bay), and **d)** VIIRS R_{rs} vs. *in situ* R_{rs} for all data (R^2 = 0.90, RMSE = 0.0007 sr^{-1}, N = 45).
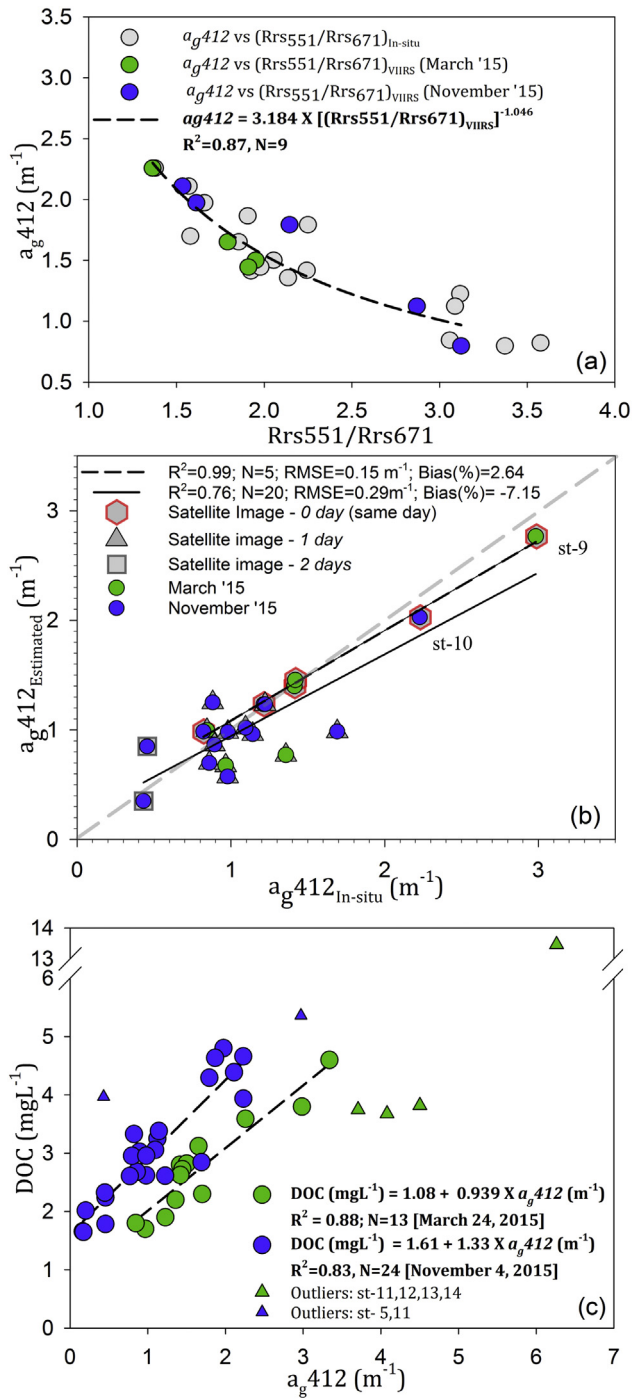
Fig. 7. a) A VIIRS based CDOM (a_g412) empirical algorithm ($R^2 = 0.87$, $N = 9$), **b)** Validation of VIIRS a_g412 against *in situ* observed a_g412 ($R^2 = 0.76$, $N = 20$, RMSE $= 0.29$ m^{-1}, Bias (%) $= -7.15$) [The symbols indicated time difference between the *in situ* observations and the satellite overpass in days, *e.g.*, hexagons – 0 day, triangles – 1 day, and squares – 2 days], and **c)** a_g412 - DOC relationships for March ($R^2 = 0.88$, $N = 13$) and November ($R^2 = 0.83$, $N = 24$) [Triangles are representing the outliers (st-5, st-11, and three stations in the East Bay) and not used in the relationships].

3.3. Major hydrodynamic forcings in Apalachicola Bay

Apalachicola River discharge was approximately two-fold higher in the wet season (March 23–25, 2015) than in the dry season (November 2–4, 2015) (Fig. 8a & b). Furthermore, the river discharge increased progressively in March, whereas it was more stable in November except after November 4, 2015. The predicted tidal-heights showed relatively

similar micro-tidal environment during both surveys; however, the ebb-tidal periods were much stronger in March than in November (Fig. 8c & d). Weak to average winds were observed during the field measurements (2.85 ± 0.97 ms^{-1} in March and 2.29 ± 1.68 ms^{-1} in November). Nonetheless, sustained periods of cold-northerly winds in March and warm-southerly winds in November could have affected the field and satellite measurements at some stations, *e.g.*, by sediment re-suspension and elevated sea-state (black boxes, Fig. 8e & f). Tidal forcing was likely the major factor controlling diurnal variation in salinity and water-level during both seasons (Fig. 8c & d). Moreover, moderate winds could have affected salinity and water-level above the tidal-height either by dispersing river-water towards the bay or by introducing shelf-water into the bay (*e.g.*, black boxes in Fig. 8) (Huang et al., 2002a; Huang et al., 2002b). Dry Bar and Cat Point salinity stations were located close to the river mouth (Fig. 1); however, they showed considerable variations in salinity during the study period (Fig. 8g & h).

3.4. Relationships between salinity, CDOM, and DOC

3.4.1. a_g412 – salinity and DOC – salinity relationships

The relationships between a_g412, DOC concentration, and salinity indicated a strong influence of terrigenous and marsh inputs (*e.g.*, the Apalachicola River (AR), the Carrabelle River (CR), and surrounding marshes) at the fresh- and marine- end members in Apalachicola Bay. Waters of different salinities such as fresh water in the river-influenced East and Central bays, brackish water in St. George Sound, and marine water just outside the bay were observed (also see Fig. 9). a_g412 and DOC concentrations near the river-influenced stations ranged from 2.26 to 6.26 m^{-1} and 3.59 to 13.47 mg L^{-1}, respectively in March (salinity <5, $n = 6$), whereas they ranged from 1.79 to 2.97 m^{-1} and 4.30 to 5.36 mg L^{-1}, respectively in November (salinity <17, $n = 7$) (Figs. 9a & 9b; Table 1). Generally, a conservative mixing of only two end-members (*e.g.*, fresh and marine) produces linear relationships between salinity and these DOM properties in most estuaries (Bauer and Bianchi, 2011). However, changing source concentration, exports from marshes, or intrusions of offshore waters could contribute to the non-conservative behavior of CDOM (Singh et al., 2010). The a_g412–salinity relationship showed a more non-conservative mixing behavior in March than in November (Fig. 9a). DOC varied linearly with salinity in March, and in November (Fig. 9b) with a steeper slope in November. However, the mean DOC concentration (2.29 ± 0.82 mg L^{-1}; St-11 was removed) in November was not significantly different (*t*-test: $p = 0.345$) than in March (3.07 ± 0.95 mg L^{-1}; St-11 & 5 were removed) despite a reduced supply of riverine- and marsh-derived DOC *via* Apalachicola River and its distributaries. Thus, pulses of river and/or marsh DOC may be rapidly attenuated or diluted in Apalachicola Bay. Station-11 was located near the marshes in East Bay (Fig. 1) that showed the highest a_g412 (6.26 and 2.97 m^{-1}) and DOC concentrations (13.47 and 5.36 mg L^{-1}) in both seasons, respectively (Figs. 9a & 9b). Despite low flow condition, the elevated a_g412 and DOC near St-5 could be due to sediment resuspension (*e.g.*, pore-water DOM) and mixing by moderate southerly winds (Fig. 8f, black box).

3.4.2. $S_{275-295}$ – salinity relationship

CDOM spectral slopes are more helpful indicators of CDOM history (*e.g.*, sources, and biological and photochemical alterations) than the absorption coefficients alone (Brown, 1977; Helms et al., 2008). Spectral slope $S_{275-295}$ ranged from (12.96 to 17.03 μm^{-1}) in March, and (16.76 to 27.73 μm^{-1}) in November. The mean $S_{275-295}$ (14.1 ± 0.89 μm^{-1}, $n = 6$) near the freshwater sources was relatively low, and slightly increased towards the saline waters in March (Fig. 9c, green symbols). In contrast, the $S_{275-295}$ showed an exponential increase from a minimum value 16.76 μm^{-1} in river to a maximum value 27.73 μm^{-1} at the shelf station in November that is typical for mixing of river water and seawater in coastal environments (Helms et al., 2008) (Fig. 9c, blue symbols). A non-linear trend of $S_{275-295}$ proved to be a good
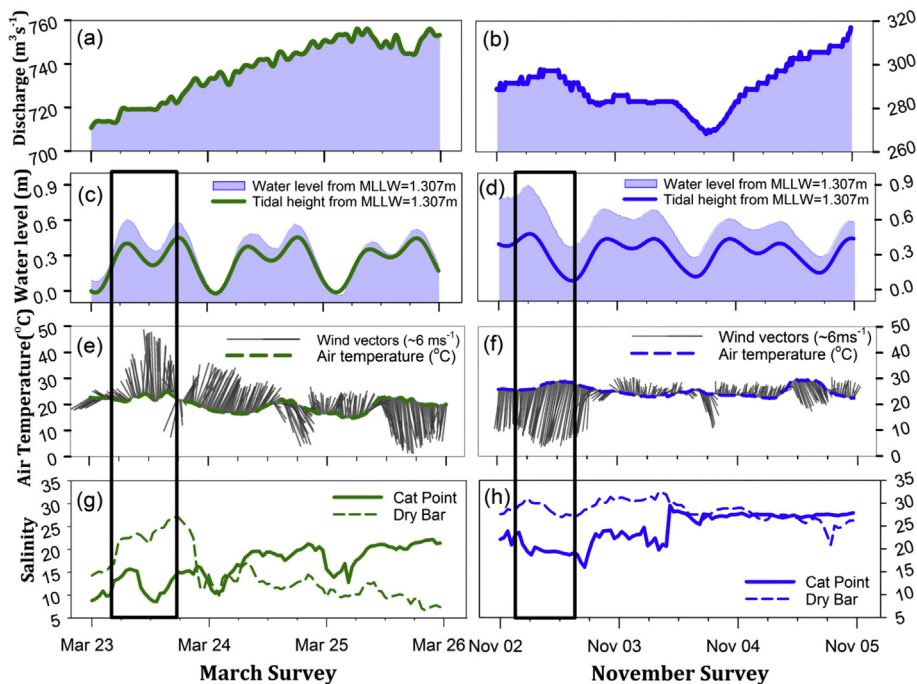
Fig. 8. Time-series of major forcing factors in Apalachicola Bay. **a–b)** Apalachicola River discharge, **c–d)** tidal-height and water-level above the datum (MLLW = 1.307 m), **e–f)** air temperature and wind vectors (wind speed and wind direction from true north), and **g–h)** salinity at Cat Point (solid line) and Dry Bar (dashed line). Black boxes show the examples of wind- and tide-affected water-level and salinity in the bay. Green color represents the wet season (March 23–25, 2015), and blue color represents the dry season (November 2–4, 2015). (For interpretation of the references to color in this figure legend, the reader is referred to the web version of this article.)

indicator of the shifts in CDOM molecular weight (MW) and photo-bleaching (Fichot and Benner, 2012; Helms et al., 2008; Vantrepotte et al., 2015; Osburn et al., 2016). Therefore, the increasing values of $S_{275–295}$ can be associated with the decrease in CDOM molecular weight and aromaticity, and the increase in photo-degradation as CDOM is transported from the fresh to marine waters. Early work has shown that under controlled laboratory conditions, photo-degradation result-ed in the breakdown of larger molecular material into smaller molecules such as fatty acids, which were rapidly consumed by bacteria (Wetzel et al., 1995). Our results indicated that Apalachicola Bay receives DOM from a variety of seasonally-dependent terrestrial and marsh sources, and their distribution can be generally governed by the interactions of various biological, physical, and photochemical processes.

3.5. Satellite-based CDOM and DOC maps in Apalachicola Bay

Atmospherically-corrected VIIRS imagery was converted to the a_g412 and DOC maps using the CDOM empirical algorithm (Eq. (6)) and a_g412-DOC relationships, respectively, and subsequently analyzed for the DOM distribution using *in situ* observations (Fig. 8) and surface currents and salinity patterns obtained from a triple nested estuarine-scale Navy Coastal Ocean Model (NCOM) at ~250 m resolution (Fig. 10).

3.6. DOC stocks and fluxes

By assuming homogeneity in DOC concentration within a pixel and shallow, vertically well-mixed water column, DOC stocks were estimat-ed from St. Vincent Sound to the East Pass for each DOC map (Fig. 11). The estimated standing stock was ~3.71×10^6 kg C (~560 km^2) on March 24, 2015 and ~4.07×10^6 kg C (~560 km^2) on November 04, 2015.

DOC fluxes calculated using water fluxes through all the passes and satellite-derived DOC concentrations for March 22–27, 2015 and No-vember 2–7, 2015 show large variations dominated by tidal cycles (Fig. 12; red lines). The de-tided DOC fluxes (Fig. 12; blue lines) were positive for both periods in spring and fall indicating export of DOC

fluxes from the bay to the coastal marine waters of the Gulf. The DOC fluxes exported out of the bay was estimated to be 6804 kg C h^{-1} (0.163×10^6 kg C d^{-1}) on March 24 and 5155.2 kg C h^{-1} (0.124×10^6 kg C d^{-1}) on November 4, 2015, respectively.

4. Discussion

4.1. Performance investigation of atmospheric-correction schemes in Apalachicola Bay

A development of ocean color algorithms for seawater constituents such as CDOM, necessitates accurate removal of the atmospheric-con-tribution (~90%) from the light observed by satellite sensors at the top-of-the-atmosphere (TOA) (Gordon and Wang, 1994). Three established correction schemes were thus evaluated, with the iterative NIR scheme (BFW10) observed to be the most suitable scheme for opti-cally complex waters of Apalachicola Bay (Fig. 5). Standard NIR-correc-tion (GW94) produced negative water-leaving radiance at short wavelengths, especially in the blue, likely due to black-pixel assumption in relatively turbid East and Central bays that could have overestimated roles of aerosols and eventually underestimated water-leaving radiance (Lavender et al., 2005; Ruddick et al., 2000; Siegel et al., 2000; Stumpf et al., 2003). However, the GW94 scheme performed reasonably well in relatively clearer shelf waters and at the green and red wavelengths, likely due to reduced atmospheric-correction errors (*e.g.*, associated with aerosol model selection using NIR bands).

Although the VIIRS SWIR bands have less noise than MODIS SWIR bands (Wang and Shi, 2012), the SWIR-correction (WS05) yielded pos-itive but overestimated values of normalized water-leaving radiance (nL_w) at all wavelengths and in different regions of the bay. The exact reason for this behavior is unknown, but the role of absorbing aerosols could be associated with the underestimation of aerosol contribution, and consequently overestimation of nL_w and R_{rs}, especially at the blue wavelength. This overcorrection may not be significant in highly turbid water where actual water-leaving signal is strong enough to conceal the over-corrected signal due to the absorbing aerosols. However, the actual
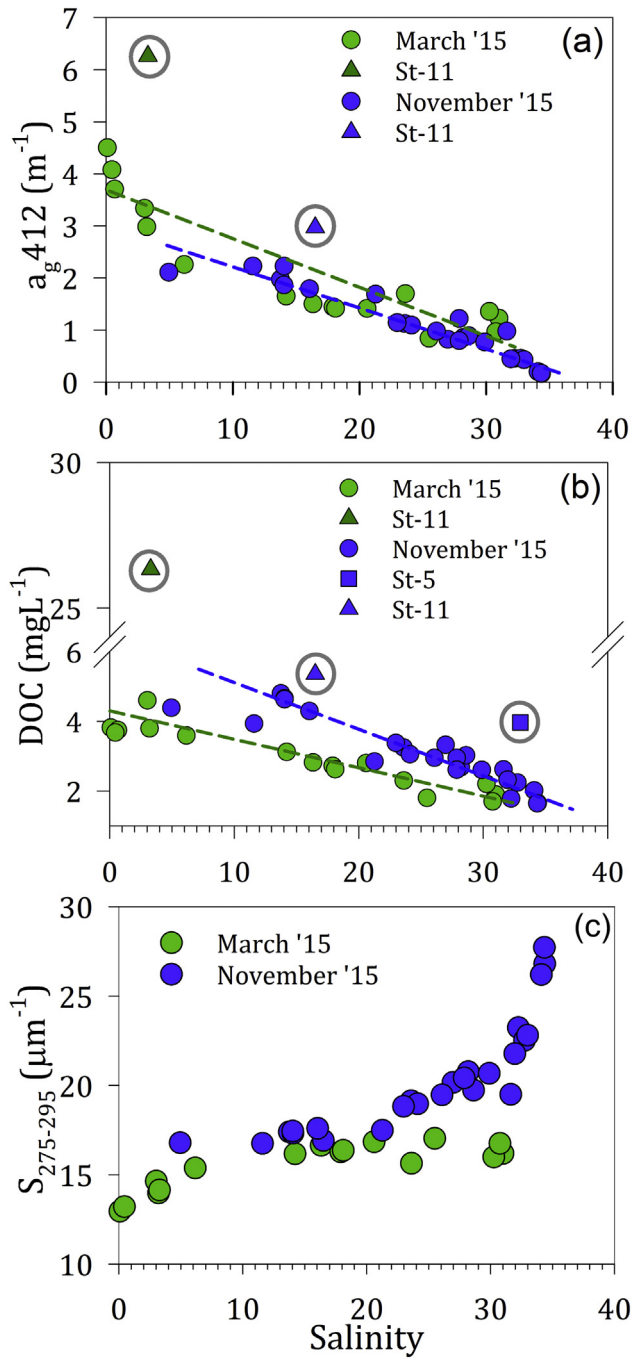
Fig. 9. Relationships between salinity and **a)** a_g412 ($a_g412 = 3.50 + 0.09 \times$ salinity, $R^2 = 0.76$, $n = 14$ in March; $a_g412 = 2.98 + 0.08 \times$ salinity, $R^2 = 0.91$, $n = 24$ in November), **b)** DOC (DOC $= 4.06–0.07 \times$ salinity, $R^2 = 0.89$, $n = 14$ in March; DOC $= 5.70–0.11 \times$ salinity, $R^2 = 0.85$, $n = 24$ in November), and **c)** $S_{275–295}$ in March (wet season; green symbols) and November (dry season; blue symbols). (For interpretation of the references to color in this figure legend, the reader is referred to the web version of this article.)

water-leaving signal may not be high enough to cause this effect in low to moderately turbid water; consequently, the over-corrected signal could be erroneously interpreted as actual water-leaving signal leading to the overestimates when compared to *in situ* observations. Another possibility is that the atmospheric-influence is also very low at SWIR wavelength, and even small uncertainties in atmospheric model selection may result in large aerosol errors (underestimation or overestimation) towards short wavelengths due to longer extrapolation distance. These errors may not have much influence in the green and red regions, but they can contribute to inaccurate (overestimated or underestimated) water-leaving radiance and *Rrs* at these wavelengths (Fig. 6). In addition, overestimated performance of the SWIR-correction can also be associated to inconsistent vicarious calibration between SWIR and visible wavelength as gain for the VIIRS SWIR bands is set to 1.0 in *l2gen* module of SeaDAS 7.3.

4.2. An empirical band ratio algorithm and a_g412 – DOC relationships

R_{rs} spectra at shorter wavelengths ($<$500 nm) are more sensitive to CDOM, hence UV and blue wavelengths can be useful in detecting CDOM in natural waters. However, the use of these wavelengths is greatly limited by negligible water-leaving radiance in blue likely due to strong CDOM absorption in CDOM-rich environments (O'Reilly et al., 2000). Furthermore, satellite retrieval errors are relatively larger in the blue region compared to longer wavelengths (*e.g.* NIR/SWIR) possibly due to the longer extrapolation distance from the red to the blue in the atmospheric correction procedure (Fig. 6b). Therefore, the blue bands were avoided in algorithm development. Zhu et al. (2014) recently reviewed 15 CDOM algorithms (empirical, semi-analytical, optimization, and matrix inversion) in Saginaw Bay (USA) and reported that three of the best performing six algorithms were empirical that used band ratios with wavelengths $>$500 nm. They further demonstrated that the band ratio performance of an empirical algorithm can be significantly improved in inland and estuarine environments by using at least one of two bands with a relatively longer wavelength ($>$600 nm). However, it is important to note that empirical band ratios are highly dependent on the dominant water constituent in the study area. Qi et al. (2015) demonstrated the use of VIIRS red to green band ratio (RGCI – red green chlorophyll index) to detect *Karenia brevis* bloom in the Northeastern Gulf of Mexico. A similar band combination worked well to detect CDOM in our study possibly due to dominance of CDOM ($a_g/a_{(total-water)} \times 100 > \sim 60\%$ at 443 nm; $a_g/a_{(total-water)} \times 100 > \sim 50\%$ at 551 nm) in Apalachicola Bay (a_g443; range $= 0.09–3.16$ m^{-1}; Mean $\pm$ SD $= 0.93 \pm 0.76$ m^{-1}) in comparison to chlorophyll concentrations during the bloom condition (a_g443; range $= 0.02–4.25$ m^{-1}; Mean $\pm$ SD $= 0.17 \pm 0.06$ m^{-1}) (Qi et al., 2015).

In situ a_g412 and VIIRS green to red band ratio ($R_{rs}551/R_{rs}671$) yielded a robust power-law relationship in Apalachicola Bay (Fig. 7a, Eq. (6)). The validation results showed a reasonable performance of this relationship for the *in situ* measurements collected within $\pm$2 days of satellite overpass (Fig. 7b). Several factors may have contributed to the observed bias in match-up comparison between *in situ* and estimated a_g412, such as errors associated with satellite TOA radiances, aerosol model selection, absorbing aerosols, *in situ* measurements, and the atmospheric-correction scheme itself. The time-difference between

Table 1
Mean, standard deviation, and range of temperature, salinity, CDOM absorption coefficient at 412 nm (a_g412) and DOC in Apalachicola Bay during two field surveys.

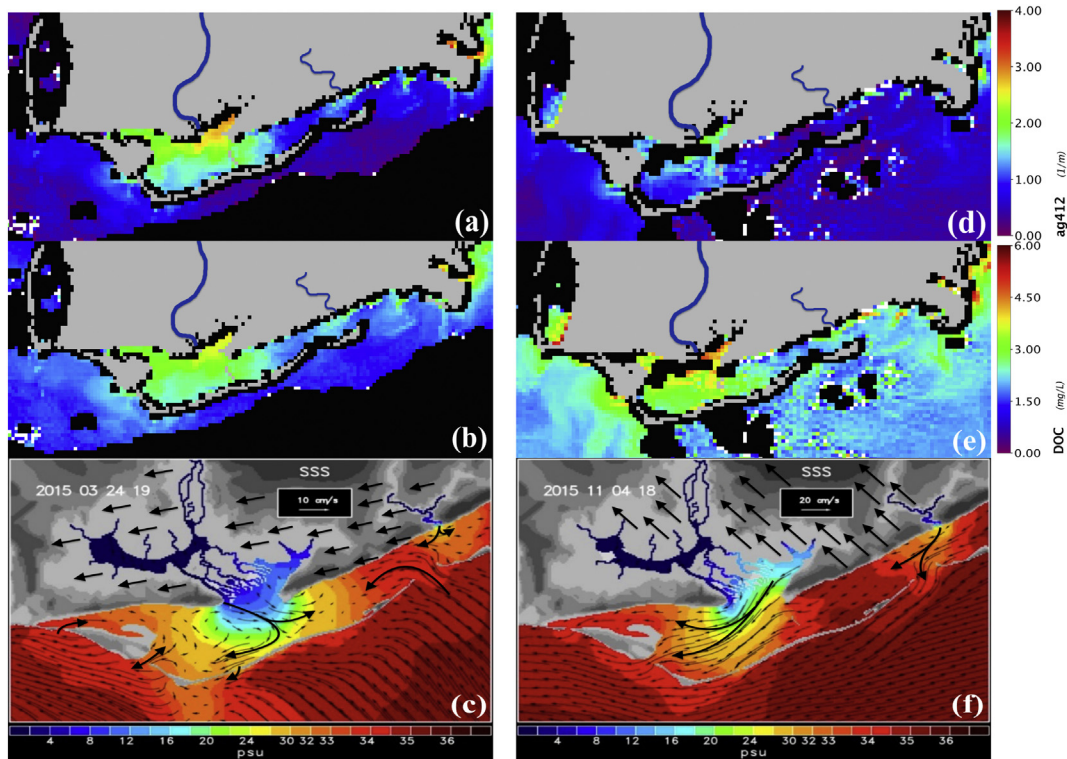| Field trips	Season	Sampling stations	Temperature (°C)	Salinity	a_g412 (m^{-1})	DOC (mg L^{-1})
March 23–25, 2015	Spring	$N = 17$	22.06 (0.78) [20.44–23.09]	15.3 (11.3) [0.09–31]	2.39 (1.51) [0.84–6.26]	4.33 (5.73) [1.7–13.47]
November 2–4, 2015	Fall	$N = 26$	25.7 (0.53) [24.6–26.3]	24.7 (8.3) [4.95–34.37]	1.15 (0.75) [0.16–2.97]	3.19 (1.03) [1.65–5.36]

Fig. 10. Synoptic views of CDOM (a_g412) and DOC concentrations during two field surveys in Apalachicola Bay. **a)** satellite-derived CDOM map, and **b)** satellite-derived DOC map, and **c)** NCOM modeled salinity and surface currents corresponding to the satellite overpass on March 24, 2015 (wet season). **d)** satellite-derived CDOM map, and **e)** satellite-derived DOC map, and **f)** NCOM modeled salinity and surface currents corresponding to the satellite overpass on November 04, 2015 (dry season). Wind direction and water transport are illustrated with black arrows in the NCOM results.

in situ and satellite observations could also produce errors in the CDOM estimation because the water characteristics can change rapidly due to major forcing factors (*e.g.*, winds, river discharge and tides; discussed later). The validation results were improved further when time-difference between the ground-truth and the satellite overpass were constrained to ±3 h (Fig. 7b) (Bailey and Werdell, 2006). Green and red channels also carry information about particle back-scattering and phytoplankton absorption, respectively. Therefore, the green to the red band ratio algorithm may not function satisfactorily in highly turbid and phytoplankton bloom conditions. Highly turbid water may mask the effect of CDOM absorption, whereas high chlorophyll-a can absorb significantly in red (Figs. 3a & 6b) that might overestimate the band ratio, and hence underestimate a_g412 (*e.g.*, st-9 & 10 located in East Bay; Fig. 7b). Variability in DOM properties, especially CDOM, likely occurs at shorter time scales in the bay due to changing terrestrial and autochthonous (planktonic) inputs, meteorological, hydrological and astronomical forcings, and DOM degradation processes such as photo-bleaching and microbial alteration. More satellite match-ups covering these variable conditions could increase the robustness of the CDOM empirical relationship in Apalachicola Bay. Finally, the a_g412–DOC relationships in March and November (Fig. 7c; Eqs. (7) & (8)) allowed for reliable satellite-derived DOC maps for the bay. While similar slope

values were observed in the relationships, different intercepts indicated the influence of different DOC sources and associated DOC removal processes during two field surveys.

4.3. Major hydrodynamic forcings in Apalachicola Bay

Major hydrodynamic forcings (winds, rivers, and tides) play a central role in regulating DOM distributions and shelf-estuarine DOM exchanges in coastal waters. Apalachicola Bay's dynamic hydrology is seasonally variable and these three forcing factors interact to control its fresh and marine water distributions. Time-series of wind speed, wind direction, air-temperature, river discharge, and tidal-height were examined together with salinity and water-level to understand the relative effects of these factors on spatiotemporal variations in the DOM properties (*e.g.*, a_g412 and DOC) during seasonally-different field surveys (Fig. 8). Winds and tides contributed the most (>50%) to the short-term variations in water-level (*e.g.*, hours to days) near the river mouth, however river discharge may exert considerable influence over the larger time-scales, *e.g.*, weeks to months (Fig. 8c & d). A combination of wind, river plume, and tidal interactions appeared to control the short-term spatial distribution of salinity in Apalachicola Bay
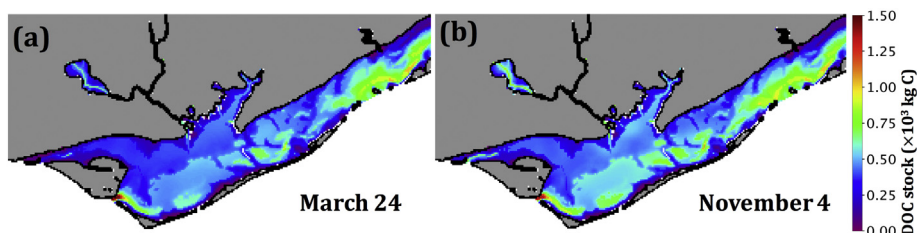

Fig. 11. Image-based standing stocks of DOC on a) March 24, 2015, and b) November 4, 2015 over a surface area of ~560 km².
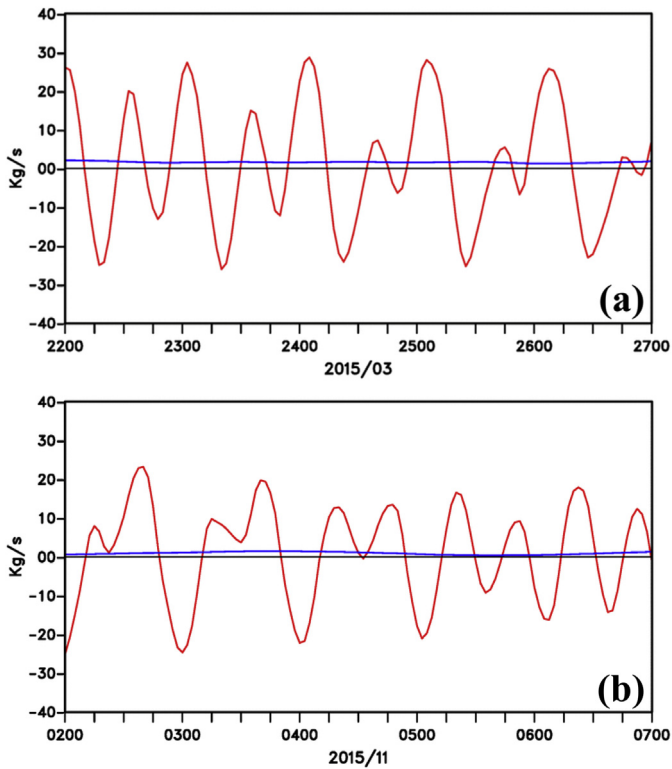
Fig. 12. Hourly DOC fluxes through the bay passes (red line; positive - out of Bay and negative into the Bay) with large variations predominated by the tides for (a) March 22–27, 2015, and (b) November 2–7, 2015. Blue lines denote estimates of de-tided (40-h filter) DOC fluxes with values of 6804 kg h^{-1} for March 24, and 5155.2 kg h^{-1} for November 4, 2015, at 12 UTC, respectively. (For interpretation of the references to color in this figure legend, the reader is referred to the web version of this article.)

based on the observed differences in salinity at the CP and DB stations (Dulaiova and Burnett, 2008; Huang et al., 2002a; Huang et al., 2002b).

Apalachicola Bay experienced low to moderate winds during the field surveys, yet sustained periods of cold-northerly winds in combination with the ebb-tidal periods likely decreased salinity by pushing river water into the bay and veering plume water towards the downwind region of the bay (Liu and Huang, 2009). One outcome of wind direction and intensity may have been to suppress outwelling of marsh-derived DOM during low river flow periods and, instead, possibly to release DOM from sediment pore-waters (Dixon et al., 2014). In contrast, a combination of warm-southerly winds and flood tidal periods were likely to introduce saline shelf water into the bay, and confine fresh water close to its sources (Chen et al., 2009). This short-term variability (*e.g.*, hours to days) in the bay's water-circulation affected allochthonous and autochthonous characteristics of DOM, their distribution, and DOM transport to the Gulf waters during the study period.

4.4. Relationships between salinity, CDOM, and DOC

4.4.1. $a_g 412$ – salinity relationship

The non-conservative behavior of CDOM likely occurred due to elevated inputs of DOM from different terrestrial sources at freshwater end-members and marsh sources at marine end-members, or to longer exposure of newly introduced CDOM to degradative processes in March (Fig. 9a, green symbols). Studies using radium isotopes (^{223}Ra and ^{224}Ra) (Dulaiova and Burnett, 2008) and 3-D hydrodynamic modeling (Mortazavi et al., 2001) showed dependence of the bay's water-circulation and residence-time on river discharge, and indicated that prevailing winds and tidal patterns can also diminish the influence of river by controlling the plume dynamics in the bay. This may, in fact, also affect the relative importance of marsh DOM export to the bay.

Moreover, an approximate flushing-time of 6 to 12 days for Apalachicola Bay was estimated, which could vary based on the combinations of river discharge, tides, and winds. The bay experienced tidal-flooding associated with semi-diurnal neap tides during the field survey in March (Fig. 8c), and that could have increased the water-flushing time in the bay. Also, the convex-shaped $a_g 412$-salinity relationship indicated a longer exposure of Central Bay and St. George Sound to CDOM removal processes (Bauer and Bianchi, 2011; D'Sa and DiMarco, 2009; Osburn et al., 2009; Osburn et al., 2016). However, a similar convex pattern could be produced by mixing of multiple end-members (Osburn and Stedmon, 2011; Osburn et al., 2016). Northerly winds were dominant during the high flow condition; hence wind-induced CDOM released from sediments due to re-suspension and mixing could also be another reason for the observed high CDOM in relatively shallow East Bay, and consequently the observed non-conservative behavior in March (Dixon et al., 2014). In contrast, a conservative mixing behavior was observed in November; however, few marine end-members showed elevated $a_g 412$ likely due to moderate southerly winds that were observed on the first day of survey in November (Fig. 8f, black box).

4.4.2. DOC – salinity relationship

The DOC – salinity relationships showed a strong conservative behavior in March and November; however, the mean DOC concentration in November was relatively similar to March despite the reduced AR and CR flows, and weak winds (Fig. 9b). The bay experienced a local precipitation event on November 3, 2015, and marsh-derived "blue carbon" might have been released into the bay due to rainfall and associated run-off during this event (Chen et al., 2011a; Chen et al., 2011b). Likewise, the fluvial concentration and flux of terrestrially-derived DOM (*e.g.*, lignin phenols) have been shown to increase rapidly during rainfall events in other settings (Ward et al., 2012). Episodic events leading to substantial DOM exports does complicate binary mixing models and may require ternary mixing models to fully elucidate terrestrial, marsh, and marine sources (Osburn and Stedmon, 2011).

4.4.3. $S_{275-295}$ – salinity relationship

The variation in the spectral slopes can be attributed to many processes *e.g.*, mixing, photo-degradation, microbial degradation, autochthonous production, pore-water supply, and flocculation. In Apalachicola Bay in March, an excess supply of riverine- and marsh-derived DOM could be the influential factor for the observed low $S_{275-295}$ in East Bay. In November, reduced freshwater inputs and longer residence-time could have exposed CDOM in the bay to photochemical and microbial oxidation processes for a period long enough to result in the higher $S_{275-295}$ in near the freshwater sources compared to March (Fig. 9c). This result would be consistent with the rapid increase in $S_{275-295}$ towards the marine end-members observed in other estuaries and coastal waters (Fichot and Benner, 2012; Helms et al., 2008).

4.5. Satellite-based CDOM and DOC maps in Apalachicola Bay

4.5.1. Wet season (March 24, 2015)

In March, higher amounts of CDOM ($a_g 412$) were observed near the river and in East Bay that gradually decreased towards the marine stations (Fig. 10a). Despite high river flow conditions, CDOM was mainly confined to Central Bay and St. Vincent Sound to the west, and low CDOM bay or Gulf water was observed in St. George Sound to the east. Furthermore, a clear westward signal of moderate CDOM observed near the mouth of Carrabelle River that indicated the net westward transport of CDOM-rich freshwater on March 24, 2015.

DOC is one of the largest pools of carbon in the biosphere whereas CDOM is an optically-reactive fraction of DOC. The extent of DOC distribution was much larger than CDOM as observed in the CDOM and DOC maps (Fig. 10b). In March, moderate DOC concentrations were observed in CDOM-depleted St. George Sound and even in the shelf waters. The strong and clearly visible westward plumes (*e.g.*, the AR and CR plumes)

of high DOC concentrations suggested the westward transport of DOM in the bay. Apalachicola Bay experienced the beginning of flooding-phase of a semi-diurnal neap tide (1900 UTC) during the satellite over-pass (1854 UTC) in March (Fig. 8c). NCOM modeling results indicated the intrusion of a saline water mass (30–34 PSU) through the West, East, and Indian Passes, and relatively weak currents (1–5 cms^{-1}) in St. George Sound and Central Bay (Fig. 10c). The presence of an anti-cy-clonic feature corresponding to reversal of surface currents near the river plume was also apparent. Although there was a net water trans-port into the bay due to flooding-phase, the tidal currents could have di-minished during the relaxation period associated with a neap tide (Fig. 8c). Nonetheless, Apalachicola River discharge was high enough to in-fluence the water-dynamics near the river plume that might have diverted fresh water towards the West Pass and St. George Sound with an anti-cyclonic distribution of surface currents in Central Bay (Fig. 10c). This phenomenon could be responsible for the observed CDOM-depleted saline water and weak surface currents in St. George Sound and Central Bay due to increased residence time and fresh- and marine water mixing. In addition, the bay experienced a shift in wind di-rections from northeasterly to southwesterly that could have contribut-ed to the net fresh river water transport towards Dry Bar (DB), and input of saline Gulf water to Cat Point (CP) through St. George Sound and the East Pass (Fig. 8e).

4.5.2. Dry season (November 4, 2015)

CDOM concentrations were lower in November 2015 compared to March 2015 and mainly restricted close to the terrestrial sources (Fig. 10d). However, despite reduced river flow and weak winds, DOC con-centration was significantly higher and stretched over a wider extent in November than in March possibly due to the strong surface currents and associated net water transport towards the shelf (Fig. 10e and f). Higher DOC concentrations could have been observed due to a marsh-derived DOC release after the traceable rainfall event that occurred a day before the satellite-overpass (1831 UTC). Time-series of dominant forcing factors (Fig. 8) and modeling results (Fig. 10f) showed a combi-nation of increasing river discharge, strong ebb tidal currents, and southeasterly winds that collectively could have veered the freshwater plume towards the western part of the bay and also supported the es-cape of freshwater to the shelf thought the West Pass and the Indian Pass.

4.6. DOC stocks and fluxes

The estimated DOC standing stock was ~10% higher on November 04, 2015 than on March 24, 2015 possibly due to terrestrial- and marsh- derived DOC-release as indicated earlier with observed higher DOC concentrations in the fall. Recent work in the Gulf of Maine esti-mated standing stock of DOC ~1.5 × 10^{10} kg C over a relatively larger area of ~90,700 km^2 (Balch et al., 2016). Although the estimates in this study may not represent accurate standing stocks of DOC because of underlying assumption of vertical homogeneity, coarse images (750 m resolution) and missing data for cloud- and stray light- masked pixels, they may provide a reasonable estimation about seasonally var-iable carbon stocks in relatively smaller Apalachicola Bay. The de-tided volume fluxes (current × area of cross-section on the all passes in m^3 s^{-1}) of water out of the bay in the spring wet season (e.g., March 24th) was 735 m^3 s^{-1} and in the fall dry season (e.g., November 4th) was 378 m^3 s^{-1}; both values closely correspond to the Apalachicola river discharge (~740 m^3 s^{-1} and ~350 m^3 s^{-1}, respectively). The vol-ume flux in the spring is more than double the fall volume flux but the DOC flux had much less of an increase (1.89 kg C s^{-1} vs. 1.43 kg C s^{-1}) (Fig. 12), which indicates a larger DOC concentration in the fall, consistent with our satellite observations (Fig. 10) and DOC stock estimates (Fig. 11). For perspective, our export values represent 7% and 21% of the 110-year mean spring and fall export values recently computed for the Mississippi River (Ren et al., 2016).

4.7. Effect of bottom reflectance on a$_g$412 and DOC stock estimations

Apalachicola River is the major source of sediments in the bay other than occasional wind- and tide- supported sediment resuspension. Ba-thymetry survey in the bay showed that Central Bay and St. George Sound are relatively deeper (>3 m) than St. Vincent Sound and East Bay (<2 m) (Twichell et al., 2010). Although East Bay is shallow, it is an optically deep region that is under continuous influence of CDOM-rich dark water and river-supplied sediment-rich water. Furthermore, sediment-resuspension is more common due to water momentum of river and its distributaries. Hence, bottom reflectance may not play a significant role in contributing to water-leaving light in East Bay. How-ever, it could be a major problem in St. Vincent Sound and near oyster bars that generally rise 2–3 m above the surrounding sea floor. None-theless, these areas become quite turbid during high flow conditions (e.g., the Apalachicola River flood) and strong winds (e.g., cold fronts and hurricanes) (Chen et al., 2009; Liu and Huang, 2009). The VIIRS CDOM algorithm is developed using in situ data collected in relatively deeper part of the bay (Central Bay), therefore low bottom contamina-tion to water-leaving light can be expected in the relationship. The bay generally remains relatively turbid during high flow conditions (e.g., in March) and hence the bottom reflectance might not be the major factor in the estimated a$_g$412 in March. However, it may have some influence on water column in St. Vincent Sound and over the oys-ter reefs and therefore on the estimated a$_g$412 and DOC stock in Novem-ber as it is the low flow condition with relatively weak winds.

5. Conclusions

This study presented the use of VIIRS ocean color sensor to monitor DOM properties, namely CDOM and DOC in the low to moderately tur-bid shallow-water estuary. It was supported by in situ observations of CDOM absorption coefficient (a$_g$412) and DOC concentrations obtained during field surveys in March and November 2015. The relationships between a$_g$412, DOC concentration and salinity indicated strong season-al influences of terrigenous and marsh inputs, such as the Apalachicola and Carrabelle Rivers, and surrounding marshes, on the DOM distribu-tions in Apalachicola Bay. A non-conservative behavior of CDOM oc-curred in March most likely due to elevated inputs of DOM from terrestrial sources and longer residence time, whereas the conservative mixing behavior was observed in November. The DOC – salinity rela-tionship showed a strong conservative behavior in March and in No-vember. Low CDOM spectral slopes in the UV indicated dominance of the source processes (e.g., elevated terrestrial inputs, autochthonous production, and wind-induced sediment re-suspension) in March, whereas larger values and a sharp increase towards the marine end-members pointed to a stronger influence of sink processes (e.g., photo-bleaching, microbial-degradation, mixing, and flocculation) (Fig. 9c). A conservative behavior was observed between CDOM and DOC during both the field surveys; however, different intercepts in their relationships indicated the seasonal-dependence of the DOM sources (e.g., riverine DOM and marsh-derived blue carbon) in March and November. On-going work on DOM biogeochemistry in this region will elucidate these sources.

Three well-known atmospheric correction schemes were tested and the iterative NIR scheme (Bailey et al., 2010) was found to be more suit-able than the standard NIR correction (Gordon and Wang, 1994), and the SWIR correction (Wang and Shi, 2005) in Apalachicola Bay. In situ a$_g$412 and atmospheric-corrected VIIRS band ratio (Rrs551/Rrs671) yielded high correlation (R^2 = 0.87) and validation showed good per-formance (R^2 = 0.76, RMSE = 0.29 m^{-1}) in the low to moderately tur-bid Apalachicola Bay. Subsequently, satellite images were converted to the CDOM and DOC maps using VIIRS-based empirical algorithm and CDOM-DOC relationships. Although some uncertainty exists in VIIRS-based CDOM empirical relationship and CDOM-DOC relationships, sat-ellite-derived CDOM and DOC maps captured major details of their

distribution and influence of season-dependent terrestrial DOM sources. The empirical relationships can be further improved by using more satellite match-ups and *in situ* measurements. Finally, satellite maps, *in situ* observations, and model-based estimation of surface currents and salinity provided a detailed view of the interactions between three major forcings (*e.g.* river, tide, and wind) and their influence on the a_g412 and DOC distribution in Apalachicola Bay. The bay experienced flood tides, northeasterly winds, net westward water transport, anti-cyclonic water circulation features, and low CDOM bay or Gulf waters in St. George Sound on March 24, 2015, whereas the time-series of dominant forcing factors and modeling results showed a combination of increasing river discharge, strong ebb tidal currents, and southeasterly winds that could have veered the freshwater plume towards the western part of the bay and also supported the escape of freshwater to the shelf thought the West Pass and Indian Pass. DOC stocks indicated that the standing stock of DOC was ~3.71×10^6 kg C in wet season, but local rainfall events may introduce "blue carbon" that could be responsible for large DOC stocks even in dry season (~4.07×10^6 kg C) in Apalachicola Bay. Nonetheless, estimates of fluxes obtained by combining NCOM hydrodynamic model currents with satellite DOC estimates indicated greater fluxes of DOC exported into the shelf waters from the bay in the wet season than the dry season that could be attributed to greater water volume fluxes and enhanced river discharged. However, reduction of DOC flux in the fall is much less than the reduction of volume flux due to relatively higher DOC concentration in the fall. Regardless, we estimate DOC exports roughly 10% of that delivered seasonally by the Mississippi River.

This study demonstrated the combined use of ocean color satellite, field observations, and hydrodynamic-modeling techniques to study influences of physical processes on the distribution and the transport of terrestrially derived CDOM and DOC to shelf waters. Satellite-derived CDOM and DOC maps showed reasonable results that matched field- and model-based observations indicating that this study can be used as a building block to calculate carbon fluxes and to recognize the role of Apalachicola Bay in the carbon cycle of the Gulf.

Acknowledgement

References

Ahmad, Z., Franz, B.A., McClain, C.R., Kwiatkowska, E.J., Werdell, J., Shettle, E.P., Holben, B.N., 2010. New aerosol models for the retrieval of aerosol optical thickness and normalized water-leaving radiances from the SeaWiFS and MODIS sensors over coastal regions and open oceans. Appl. Opt. 49, 5545–5560.

Bailey, S.W., Franz, B.A., Werdell, P.J., 2010. Estimation of near-infrared water-leaving reflectance for satellite ocean color data processing. Opt. Express 18, 7521–7527.

Bailey, S.W., Werdell, P.J., 2006. A multi-sensor approach for the on-orbit validation of ocean color satellite data products. Remote Sens. Environ. 102, 12–23.

Balch, W., Huntington, T., Aiken, G., Drapeau, D., Bowler, B., Lubelczyk, L, Butler, K., 2016. Toward a quantitative and empirical dissolved organic carbon budget for the Gulf of Maine, a semienclosed shelf sea. Glob. Biogeochem. Cycles 30, 268–292.

Bauer, J., Bianchi, T., 2011. 5.02—dissolved organic carbon cycling and transformation. In: Wolanski, E., DS, McLusky (Eds.), Treatise on Estuarine and Coastal Science 5. Academic Press, Waltham, pp. 7–67.

Bauer, J.E., Cai, W.-J., Raymond, P.A., Bianchi, T.S., Hopkinson, C.S., Regnier, P.A., 2013. The changing carbon cycle of the coastal ocean. Nature 504, 61–70.

Bianchi, T.S., 2007. Biogeochemistry of Estuaries. Oxford University Press (720 pp).

Bianchi, T.S., DiMarco, S.F., Smith, R.W., Schreiner, K.M., 2009. A gradient of dissolved organic carbon and lignin from Terrebonne–Timbalier Bay estuary to the Louisiana shelf (USA). Mar. Chem. 117, 32–41.

Borges, A., Delille, B., Frankignoulle, M., 2005. Budgeting sinks and sources of CO_2 in the coastal ocean: diversity of ecosystems counts. Geophys. Res. Lett. 32.

Brown, M., 1977. Transmission spectroscopy examinations of natural waters: C. Ultraviolet spectral characteristics of the transition from terrestrial humus to marine yellow substance. Estuar. Coast. Mar. Sci. 5, 309–317.

Chaichitehrani, N., D'Sa, E.J., Ko, D.S., Walker, N.D., Osburn, C.L., Chen, R.F., 2014. Colored dissolved organic matter dynamics in the northern Gulf of Mexico from ocean color and numerical model results. J. Coast. Res. 30, 800–814.

Chen, S., Huang, W., Chen, W., Chen, X., 2011a. An enhanced MODIS remote sensing model for detecting rainfall effects on sediment plume in the coastal waters of Apalachicola Bay. Mar. Environ. Res. 72, 265–272.

Chen, S., Huang, W., Chen, W., Wang, H., 2011b. Remote sensing analysis of rainstorm effects on sediment concentrations in Apalachicola Bay, USA. Ecol. Inf. 6, 147–155.

Chen, S., Huang, W., Wang, H., Li, D., 2009. Remote sensing assessment of sediment resuspension during Hurricane Frances in Apalachicola Bay, USA. Remote Sens. Environ. 113, 2670–2681.

D'Sa, E.J., 2008. Colored dissolved organic matter in coastal waters influenced by the Atchafalaya River, USA: effects of an algal bloom. J. Appl. Remote. Sens. 2, 023502–023511.

D'Sa, E.J., DiMarco, S.F., 2009. Seasonal variability and controls on chromophoric dissolved organic matter in a large river-dominated coastal margin. Limnol. Oceanogr. 54 (6), 2233–2242.

D'Sa, E.J., Goes, J.I., Gomes, H., Mouw, C., 2014. Absorption and fluorescence properties of chromophoric dissolved organic matter of the eastern Bering Sea in the summer with special reference to the influence of a cold pool. Biogeosciences 11, 3225–3244.

D'Sa, E.J., Ko, D.S., 2008. Short-term influences on suspended particulate matter distribution in the northern Gulf of Mexico: satellite and model observations. Sensors 8, 4249–4264.

D'Sa, E.J., Miller, R.L., 2003. Bio-optical properties in waters influenced by the Mississippi River during low flow conditions. Remote Sens. Environ. 84, 538–549.

D'Sa, E.J., Miller, R.L., Del Castillo, C., 2006. Bio-optical properties and ocean color algorithms for coastal waters influenced by the Mississippi River during a cold front. Appl. Opt. 45, 7410–7428.

Del Castillo, C.E., Miller, R.L., 2008. On the use of ocean color remote sensing to measure the transport of dissolved organic carbon by the Mississippi River Plume. Remote Sens. Environ. 112, 836–844.

Del Vecchio, R., Blough, N.V., 2004. Spatial and seasonal distribution of chromophoric dissolved organic matter and dissolved organic carbon in the Middle Atlantic Bight. Mar. Chem. 89, 169–187.

Dixon, J.L., Osburn, C.L., Paerl, H.W., Peierls, B.L., 2014. Seasonal changes in estuarine dissolved organic matter due to variable flushing time and wind-driven mixing events. Estuar. Coast. Shelf Sci. 151, 210–220.

Dulaiova, H., Burnett, W.C., 2008. Evaluation of the flushing rates of Apalachicola Bay, Florida via natural geochemical tracers. Mar. Chem. 109, 395–408.

Edmiston, H.L., 2008a. A River Meets the bay: a Characterization of the Apalachicola River and Bay system. Apalachicola National Estuarine Research Reserve (ANERR). Available at. http://www.dep.state.fl.us/coastal/downloads/management_plans/A_River_Meets_the_Bay.pdf (Accessed in December 2015).

Edmiston, H.L., Fahrny, S.A., Lamb, M.S., Levi, L.K., Wanat, J.M., Avant, J.S., Wren, K., Selly, N.C., 2008b. Tropical storm and hurricane impacts on a Gulf Coast estuary: Apalachicola Bay, Florida. J. Coast. Res. 38–49.

Fellman, J.B., Hood, E., Edwards, R.T., D'Amore, D.V., 2009. Changes in the concentration, biodegradability, and fluorescent properties of dissolved organic matter during stormflows in coastal temperate watersheds. J. Geophys. Res. Biogeosci. 114.

Fichot, C.G., Benner, R., 2011. A novel method to estimate DOC concentrations from CDOM absorption coefficients in coastal waters. Geophys. Res. Lett. 38.

Fichot, C.G., Benner, R., 2012. The spectral slope coefficient of chromophoric dissolved organic matter (S275–295) as a tracer of terrigenous dissolved organic carbon in river-influenced ocean margins. Limnol. Oceanogr. 57, 1453–1466.

Fichot, C.G., Benner, R., 2014. The fate of terrigenous dissolved organic carbon in a river-influenced ocean margin. Glob. Biogeochem. Cycles 28, 300–318.

Gordon, H.R., Wang, M., 1994. Retrieval of water-leaving radiance and aerosol optical thickness over the oceans with SeaWiFS: a preliminary algorithm. Appl. Opt. 33, 443–452.

Gould Jr., R., Arnone, R., Sydor, M., 2001. Absorption, scattering, and remote-sensing reflectance relationships in coastal waters: testing a new inversion algorithm. J. Coast. Res. 328–341.

Grattan, L.M., Roberts, S., Mahan Jr., W.T., McLaughlin, P.K., Otwell, W.S., Morris Jr., J.G., 2011. The early psychological impacts of the Deepwater Horizon oil spill on Florida and Alabama communities. Environ. Health Perspect. 119, 838.

Green, S.A., Blough, N.V., 1994. Optical absorption and fluorescence properties of chromophoric dissolved organic matter in natural waters. Limnol. Oceanogr. 39, 1903–1916.

Hale, G.M., Querry, M.R., 1973. Optical constants of water in the 200-nm to 200-μm wavelength region. Appl. Opt. 12, 555–563.

Hansell, D.A., Carlson, C.A., 2014. Biogeochemistry of Marine Dissolved Organic Matter. Academic Press.

Havens, K., Allen, M., Camp, E., Irani, T., Lindsey, A., Morris, J., Kane, A., Kimbro, D., Otwell, S., Pine, B., 2013. Apalachicola Bay Oyster Situation Report. Florida Sea Grant College Program, Technical Publication TP-200.

Hedges, J.I., Hatcher, P.G., Ertel, J.R., Meyers-Schulte, K.J., 1992. A comparison of dissolved humic substances from seawater with Amazon River counterparts by ^{13}C-NMR spectrometry. Geochim. Cosmochim. Acta 56, 1753–1757.

Helms, J.R., Stubbins, A., Ritchie, J.D., Minor, E.C., Kieber, D.J., Mopper, K., 2008. Absorption spectral slopes and slope ratios as indicators of molecular weight, source, and photobleaching of chromophoric dissolved organic matter. Limnol. Oceanogr. 53, 955–969.

Hu, C., Carder, K.L., Muller-Karger, F.E., 2000. Atmospheric correction of SeaWiFS imagery over turbid coastal waters: a practical method. Remote Sens. Environ. 74, 195–206.

Huang, W., Jones, W., Wu, T., 2002a. Modelling wind effects on subtidal salinity in Apalachicola Bay, Florida. Estuar. Coast. Shelf Sci. 55, 33–46.

Huang, W., Sun, H., Nnaji, S., Jones, W., 2002b. Tidal hydrodynamics in a multiple-inlet estuary: Apalachicola Bay, Florida. J. Coast. Res. 674–684.

Huguet, A., Vacher, L., Relexans, S., Saubusse, S., Froidefond, J.-M., Parlanti, E., 2009. Properties of fluorescent dissolved organic matter in the Gironde estuary. Org. Geochem. 40, 706–719.

Jaffé, R., Boyer, J., Lu, X., Maie, N., Yang, C., Scully, N., Mock, S., 2004. Source characterization of dissolved organic matter in a subtropical mangrove-dominated estuary by fluorescence analysis. Mar. Chem. 84, 195–210.

Jerlov, N.G., 1976. Marine Optics. Elsevier.

Joshi, I., D'Sa, E.J., 2015. Seasonal variation of colored dissolved organic matter in Barataria Bay, Louisiana, using combined Landsat and field data. Remote Sens. 7, 12478–12502.

Jurado, E., Dachs, J., Duarte, C.M., Simó, R., 2008. Atmospheric deposition of organic and black carbon to the global oceans. Atmos. Environ. 42, 7931–7939.

Kirk, J.T., 1994. Light and Photosynthesis in Aquatic Ecosystems. Cambridge university press.

Ko, D.S., Martin, P.J., Rowley, C.D., Preller, R.H., 2008. A real-time coastal ocean prediction experiment for MREA04. J. Mar. Syst. 69, 17–28.

Koch, M., Sun, H., 1999. Tidal and non-tidal characteristics of water levels and flow in the Apalachicola Bay, Florida. In: Brebbia, C.A., Anagnostpolous, P. (Eds.), Coastal Engineering and Marina Developments. WIT Press, Southampton, UK, pp. 357–366.

Lavender, S., Pinkerton, M., Moore, G., Aiken, J., Blondeau-Patissier, D., 2005. Modification to the atmospheric correction of SeaWiFS ocean colour images over turbid waters. Cont. Shelf Res. 25, 539–555.

Lehrter, J., Ko, D.S., Murrell, M., Richard, G., James, H., Blake, S., Gould, R.W., Penta, B., 2013. Nutrient transports and source/sink dynamics on the inner Louisiana continental shelf. J. Geophys. Res. 118, 4822–4838.

Lee, Z., Carder, K.L., Steward, R.G., Peacock, T.G., Davis, C.O., Mueller, J.L., 1997. Remote sensing reflectance and inherent optical properties of oceanic waters derived from above-water measurements. Ocean Optics XIII. International Society for Optics and Photonics, pp. 160–166.

Liu, X., Huang, W., 2009. Modeling sediment resuspension and transport induced by storm wind in Apalachicola Bay, USA. Environ. Model Softw. 24, 1302–1313.

Livingston, R.J., 2014. Climate Change and Coastal Ecosystems: Long-Term Effects of Climate and Nutrient Loading on Trophic Organization. CRC Press.

Livingston, R.J., Niu, X., Lewis III, F.G., Woodsum, G.C., 1997. Freshwater input to a Gulf estuary: long-term control of trophic organization. Ecol. Appl. 7, 277–299.

Loisel, H., Vantrepotte, V., Dessailly, D., Mériaux, X., 2014. Assessment of the colored dissolved organic matter in coastal waters from ocean color remote sensing. Opt. Express 22, 13109–13124.

Mannino, A., Russ, M.E., Hooker, S.B., 2008. Algorithm development and validation for satellite-derived distributions of DOC and CDOM in the US Middle Atlantic Bight. J. Geophys. Res. Oceans 113.

McCarthy, M.D., Hedges, J.I., Benner, R., 1998. Major bacterial contribution to marine dissolved organic nitrogen. Science 281, 231–234.

McCarthy, S.C., Gould, R.W., Richman, J., Kearney, C., Lawson, A., 2012. Impact of aerosol model selection on water-leaving radiance retrievals from satellite ocean color imagery. Remote Sens. 4, 3638–3665.

Mobley, C.D., 1999. Estimation of the remote-sensing reflectance from above-surface measurements. Appl. Opt. 38, 7442–7455.

Mortazavi, B., Iverson, R.L., Huang, W., 2001. Dissolved organic nitrogen and nitrate in Apalachicola Bay, Florida: spatial distributions and monthly budgets. Mar. Ecol. Prog. Ser. 214, 79–91.

Moyer, R.P., Powell, C.E., Gordon, D.J., Long, J.S., Bliss, C.M., 2015. Abundance, distribution, and fluxes of dissolved organic carbon (DOC) in four small sub-tropical rivers of the Tampa Bay estuary (Florida, USA). Appl. Geochem. 63, 550–562.

Mueller, J.L., Davis, C., Arnone, R., Frouin, R., Carder, K., Lee, Z., Steward, R., Hooker, S., Mobley, C.D., McLean, S., 2003. Above-Water Radiance and Remote Sensing Reflectance Measurements and Analysis Protocols. Ocean Optics Protocols for Satellite Ocean Color Sensor Validation Revision. 4 pp. 21–31.

Osburn, C.L., St-Jean, G., 2007. The use of wet chemical oxidation with high-amplification isotope ratio mass spectrometry (WCO-IRMS) to measure stable isotope values of dissolved organic carbon in seawater. Limnol. Oceanogr. Methods 5, 296–308.

Osburn, C.L., O'Sullivan, D.W., Boyd, T.J., 2009. Increases in the longwave photobleaching of chromophoric dissolved organic matter in coastal waters. Limnol. Oceanogr. 54 (1), 145–159.

Osburn, C.L., Stedmon, C.A., 2011. Linking the chemical and optical properties of dissolved organic matter in the Baltic–North Sea transition zone to differentiate three allochthonous inputs. Mar. Chem. 126, 281–294.

Osburn, C.L., Boyd, T.J., Montgomery, M.T., Bianchi, T.S., Coffin, R.B., Paerl, H.W., 2016. Optical proxies for terrestrial dissolved organic matter in estuaries and coastal waters. Front. Mar. Sci. 2 (127). http://dx.doi.org/10.3389/fmars.2015.00127.

O'Reilly, J.E., Hooker, S.B., Firestone, E.R., 2000. SeaWiFS Postlaunch Calibration and Validation Analyses (Part 3), Technical Report Series NASA Technical Memorandum 2000-206892. Vol. 11. NASA Goddard Space Flight Center, Greenbelt, MD, USA.

Qi, L., Hu, C., Cannizzaro, J., Corcoran, A.A., English, D., Le, C., 2015. VIIRS observations of a Karenia brevis bloom in the Northeastern Gulf of Mexico in the absence of a fluorescence band. IEEE Geosci. Remote Sens. Lett. 12 (11), 2213–2217.

Ren, W., Tian, H., Cai, W.J., Lohrenz, S.E., Hopkinson, C.S., Huang, W.-J., Yang, J., Tao, B., Pan, S., He, R., 2016. Century-long increasing trend and variability of dissolved organic carbon export from the Mississippi River basin driven by natural and anthropogenic forcing. Global Biogeochem. Cycles 30, 1288–1299.

Ruddick, K.G., Ovidio, F., Rijkeboer, M., 2000. Atmospheric correction of SeaWiFS imagery for turbid coastal and inland waters. Appl. Opt. 39, 897–912.

Santos, I.R., Burnett, W.C., Dittmar, T., Suryaputra, I.G.N.A., Chanton, J., 2009. Tidal pumping drives nutrient and dissolved organic matter dynamics in a Gulf of Mexico subterranean estuary. Geochim. Cosmochim. Acta 73, 1325–1339.

Schroeder, W.M., Wiseman, W.J., 1999. Geology and hydodynamics of Gulf of Mexico estuaries. In: Bianchi, T.S., Pennock, J.R., Twilley, R.R. (Eds.), Biogeochemistry of Gulf of Mexcio Estuaries. John Wiley & Sons, N.Y, pp. 3–28.

Shifrin, K., 1988. Physical Optics of Ocean Water (Springer Science & Business Media).

Siegel, D.A., Wang, M., Maritorena, S., Robinson, W., 2000. Atmospheric correction of satellite ocean color imagery: the black pixel assumption. Appl. Opt. 39, 3582–3591.

Singh, S., D'Sa, E.J., Swenson, E.M., 2010. Chromophoric dissolved organic matter (CDOM) variability in Barataria Bay using excitation-emission matrix (EEM) fluorescence and parallel factor analysis. Sci. Total Environ. 408, 3211–3222.

Sleighter, R.L., Hatcher, P.G., 2008. Molecular characterization of dissolved organic matter (DOM) along a river to ocean transect of the lower Chesapeake Bay by ultrahigh resolution electrospray ionization Fourier transform ion cyclotron resonance mass spectrometry. Mar. Chem. 110, 140–152.

Solis, R.S., Powell, G.L., 1999. Hydrology, mixing characteristics, and residence times of Gulf of Mexico estuaries. In: Bianchi, T.S., Pennock, J.R., Twilley, R.R. (Eds.), Biogeochemistry of Gulf of Mexcio Estuaries. John Wiley & Sons, N.Y, pp. 29–61.

Spencer, R.G., Ahad, J.M., Baker, A., Cowie, G.L., Ganeshram, R., Upstill-Goddard, R.C., Uher, G., 2007. The estuarine mixing behaviour of peatland derived dissolved organic carbon and its relationship to chromophoric dissolved organic matter in two North Sea estuaries (UK). Estuar. Coast. Shelf Sci. 74, 131–144.

Stumpf, R., Arnone, R., Gould, R., Martinolich, P., Ransibrahmanakul, V., 2003. A partially coupled ocean-atmosphere model for retrieval of water-leaving radiance from SeaWiFS in coastal waters. NASA Tech. Memo 206892, 51–59.

Tehrani, N.C., D'Sa, E.J., Osburn, C.L., Bianchi, T.S., Schaeffer, B.A., 2013. Chromophoric dissolved organic matter and dissolved organic carbon from sea-viewing wide field-of-view sensor (SeaWiFS), moderate resolution imaging spectroradiometer (MODIS) and MERIS sensors: Case study for the Northern Gulf of Mexico. Remote Sens. 5, 1439–1464.

Thuillier, G., Hersé, M., Foujols, T., Peetermans, W., Gillotay, D., Simon, P., Mandel, H., 2003. The solar spectral irradiance from 200 to 2400 nm as measured by the SOLSPEC spectrometer from the ATLAS and EURECA missions. Sol. Phys. 214, 1–22.

Twichell, D., Edmiston, L., Andrews, B., Stevenson, W., Donoghue, J., Poore, R., Osterman, L., 2010. Geologic controls on the recent evolution of oyster reefs in Apalachicola Bay and St. George sound, Florida. Estuar. Coast. Shelf Sci. 88, 385–394.

Vantrepotte, V., Danhiez, F.-P., Loisel, H., Ouillon, S., Mériaux, X., Cauvin, A., Dessailly, D., 2015. CDOM-DOC relationship in contrasted coastal waters: implication for DOC retrieval from ocean color remote sensing observation. Opt. Express 23, 33–54.

Wang, M., Shi, W., 2005. Estimation of ocean contribution at the MODIS near-infrared wavelengths along the east coast of the US: two case studies. Geophys. Res. Lett. 32.

Wang, M., Shi, W., 2006. Cloud masking for ocean color data processing in the coastal regions. Geosci. Remote Sens. IEEE Trans. 44, 3105–3196.

Wang, M., Shi, W., 2012. Sensor noise effects of the SWIR bands on MODIS-derived ocean color products. IEEE Trans. Geosci. Remote Sens. 50 (9), 3280–3292.

Ward, N.D., Richey, J.E., Keil, R.G., 2012. Temporal variation in river nutrient and dissolved lignin phenol concentrations and the impact of storm events on nutrient loading to Hood Canal, Washington, USA. Biogeochemistry 111, 629–645.

Wetzel, R.G., Hatcher, P.G., Bianchi, T.S., 1995. Natural photolysis by ultraviolet irradiance of recalcitrant dissolved organic matter to simple substrates for rapid bacterial metabolism. Limnol. Oceanogr. 40 (8), 1369–1380.

Whitfield, W., Beaumariage, D.S., 1977. Shellfish management in Apalachicola Bay: past, present and future. In: Livingston, R.J., Joyce, E.A. (Eds.), Proceedings of the Conference on the Apalachicola Drainage System (Held in Gainesville, FL). Florida Marine Research Publications no Vol. 26, pp. 130–140.

Wilber, D.H., 1992. Associations between freshwater inflows and oyster productivity in Apalachicola Bay, Florida. Estuar. Coast. Shelf Sci. 35, 179–190.

Zhu, W., Qian, Y., Tian, Y.Q., Becker, B.L., Zheng, T., Carrick, H.J., 2014. An assessment of remote sensing algorithms for colored dissolved organic matter in complex freshwater environments. Remote Sens. Environ. 140, 766–778.